CrossMark

JM PAPERS

Correlation function and linear response function of homogeneous isotropic turbulence in the Eulerian and Lagrangian coordinates

Takeshi Matsumoto[1],†, **Michio Otsuki**[2], **Takeshi Ooshida**[3] **and Susumu Goto**[2]

[1]Division of Physics and Astronomy, Graduate School of Science, Kyoto University, Kyoto 606-8502, Japan

[2]Graduate School of Engineering Science, Osaka University, Toyonaka 560-8531, Japan

[3]Department of Mechanical and Aerospace Engineering, Tottori University, Tottori 680-8552, Japan

We study the correlation function and mean linear response function of the velocity Fourier mode of statistically steady-state, homogeneous and isotropic turbulence in Eulerian and Lagrangian coordinates through direct numerical simulation (DNS). As the Lagrangian velocity, we here adopt Kraichnan's Lagrangian-history framework where Lagrangian particles are labelled with current positions and their velocities are measured at some time before. This Lagrangian velocity is numerically calculated with a method known as the passive vector method. Our first goal is to study the relation between the correlation function and the mean linear response function in Eulerian and Lagrangian coordinates. Such a relation is known to be important in analysing the closed set of equations for the two functions, which are obtained by direct-interaction-approximation-type closures. We demonstrate numerically that the fluctuation–dissipation theorem (proportionality between the two functions) does not hold. The relation is further investigated with general analytical expressions of the mean linear response function under stochastic settings, which are known as the fluctuation-response relations in non-equilibrium statistical mechanics. Our second goal is to identify characteristic times associated with the two functions and to compare the times between the Eulerian and Lagrangian coordinates. Our DNS result supports the common view that the Eulerian characteristic times have the sweeping-time scaling ($\propto k^{-1}$, where k is the wavenumber) for both functions and the Lagrangian characteristic times in the inertial range have the Kolmogorov-time scaling ($\propto k^{-2/3}$) for both functions.

Key words: turbulence theory, turbulence simulation

† Email address for correspondence: takeshi@koryu.scphys.kyoto-u.ac.jp

T. Matsumoto, M. Otsuki, T. Ooshida and S. Goto

1. Introduction

The two-point correlation function of the velocity in turbulence has been the central object in statistical theory of homogeneous and isotropic turbulence. In particular, one goal of the theory is to derive the functional form of the energy spectrum from the incompressible Navier–Stokes equations in Fourier space. However, due to the quadratic nonlinearity, an equation for the correlation function cannot be obtained rigorously in a closed form, which is known as the closure problem (see, e.g. Leslie 1973; Pope 2000; Davidson 2004).

To overcome this intrinsic problem, various approximations have been proposed to close the equation for the correlation function, as described critically, for example, in Davidson (2004). Among those approximations, there is an exceptional one: the direct interaction approximation (DIA) proposed by Kraichnan (1959), although the first DIA in the Eulerian coordinates failed to recover the Kolmogorov spectrum $k^{-5/3}$, where k is the wavenumber in the inertial range (see, e.g. Leslie 1973). By exceptional, it is understood that the DIA does not have any adjustable parameters and that the mean linear response function was introduced for the first time in the closure approximations of the Navier–Stokes equations (see, e.g. Marconi *et al.* 2008; Eyink & Frisch 2011). The mean linear response function, or the Green's function, which many physicists started to use in the 1950s, is now a standard theoretical device of closure approximation of the correlation function in nonlinear statistical problems (see, e.g. Frisch 1996; Marconi *et al.* 2008). Specifically, the reason for utilising the mean linear response function (linear response function for short) is to describe the nonlinear effect in a perturbative manner. In this closure framework, the linear response function and the correlation function are considered on an equal footing. Motivated by this framework, we study several important aspects of the linear response function via direct numerical simulation (DNS) in Eulerian and Lagrangian coordinates. These aspects are described in the next subsections. In particular, to our knowledge, a DNS study of the Lagrangian linear response function is reported here for the first time.

1.1. *Relation between the linear response function and the correlation function: fluctuation-response relation (FRR)*

In the DIA-type closures, one of the crucial elements is the relation between the linear response function and the correlation function. As the result of the approximations, we end up typically with a set of two closed integro-differential equations for the linear response function and the two-point correlation function. We then need to solve the set of equations numerically. In practice, we solve them simultaneously by assuming that the linear response function and the correlation function are self-similar. In this process, we often encounter difficulties such as infra-red or ultra-violet divergence of the integrals, see, e.g. a discussion concerning the mode-coupling theory of colloidal suspensions in Miyazaki & Reichman (2005) (this is not always the case for turbulence, however).

One way to circumvent this problem is to utilise an expression of the linear response function in terms of suitable correlation functions, which is called the FRR. The special case of FRR is the fluctuation-dissipation theorem (FDT): in equilibrium statistical mechanics the two functions are proportional, with the proportionality constant being the inverse temperature, see e.g. Marconi *et al.* (2008). The FDT is considered to fail generally in systems out of equilibrium. Indeed, this has been demonstrated for a number of non-equilibrium steady-state systems, as discussed in Marconi *et al.* (2008). In particular, it was shown that the FDT is invalid for forced Navier–Stokes turbulence in the dissipation range in Carini & Quadrio (2010) and for the forced Sabra shell model in our previous

work (Matsumoto *et al.* 2014). The breakdown of the FDT is surely a manifestation of the out-of-equilibrium character of turbulence and of the shell model.

There are several forms of FRRs that hold for general out-of-equilibrium cases, as reviewed in § 3 of Marconi *et al.* (2008) and also § 4 of Puglisi, Sarracino & Vulpiani (2017). Unfortunately, they are not written with the two-point or multi-point correlation functions. The most general one is written with a formal derivative of the invariant measure. Hence, they cannot be used in solving the two integro-differential equations of the correlation function and the linear response function, which are obtained by closure approximations.

However, if we add random noise to the system, the situation becomes different. In this stochastic setting, there is at least one general expression for the linear response function in terms of multi-point correlation functions, which was obtained by Harada & Sasa (2005, 2006). This recent development in non-equilibrium statistical mechanics has urged us to consider the correlation function and the linear response function of turbulence from a new perspective. This Harada–Sasa relation was the basis of our previous study (Matsumoto *et al.* 2014) to consider a similar FRR for the shell model and the Navier–Stokes equations in the Eulerian coordinates. With random noise, there is yet another general expression of the linear response function in terms of the correlation between the random noise itself and the solution. This was obtained by Novikov (1965) and was studied numerically by Carini & Quadrio (2010). We consider these two FRRs in this paper by adding a random forcing to the Navier–Stokes equations in addition to the deterministic large-scale forcing to maintain the turbulence in a statistically steady state.

Of course, such random forcing or noise does not have any physical origin in turbulent flows, whereas, for the microscopic systems considered in Harada & Sasa (2005, 2006), the Langevin noise therein has a definite physical origin as an effect of thermal fluctuations in the background environment. We regard our random forcing as a theoretical and numerical tool to investigate the response function and consider the zero limit of the random forcing (here, we do not intend to regard the randomly forced Navier–Stokes equations as a fluctuating hydrodynamic description for mesoscopic systems).

In the present study, first, we demonstrate numerically the breakdown of the FDT. Second, by adding small random forcing, we check whether the two types of non-equilibrium FRRs hold for the forced Navier–Stokes turbulence in Eulerian coordinates for the energy-containing, inertial and dissipation ranges. In particular, the Harada–Sasa relation is applied to the Navier–Stokes case for the first time. In the Lagrangian coordinates, numerical simulation of the FRRs with random forcing is almost impossible, as we will see. Hence, we only give expressions for the Lagrangian FRRs.

1.2. *Difference in the Eulerian and Lagrangian coordinates: time scale and FRR*

There is another well-known problem in the DIA-type closures of turbulence: it is understood that the failure of the earliest version of the DIA, leading to the $k^{-3/2}$ scaling of the energy spectrum in the inertial range, was due to picking up the sweeping time scale instead of the proper Kolmogorov time scale in the inertial range. This is ascribed to a lack of Galilean invariance of the velocity correlation function in Eulerian coordinates, see, e.g. Leslie (1973). The DIA in Lagrangian coordinates, called Lagrangian-history DIA (LHDIA), was later elaborated by Kraichnan (1965) who succeeded in reproducing the Kolmogorov $k^{-5/3}$ spectrum (Kraichnan 1966).

This implies that the time scales of the correlation function and the linear response function are critical factors in order to have a correct result. In other words, as discussed in

Kraichnan (1965), a correct approximation to the Kolmogorov spectrum should be capable of distinguishing between the time scales of the internal distortion caused by the flow of the same spatial scales and that of the sweeping motion without distortion caused by the flow of much larger scales. However, these time scales of the correlation function and the linear response function are not well studied numerically nor experimentally in spite of their critical role in the closures. In the present paper, we show via DNS that, indeed, the time scale of the linear response function in Lagrangian coordinates is consistent with the Kolmogorov scaling $k^{-2/3}$ for the first time (we analyse the linear response function in the Lagrangian-history framework).

Given the success of the LHDIA, more straightforward DIA-type closures in Lagrangian coordinates have been developed without *ad hoc* assumptions. Mostly, the development was to incorporate the forward-in-time (measuring time) evolution of the Lagrangian velocity field. Notable ones include the Lagrangian renormalised approximation (LRA) by Kaneda (1981) and the Lagrangian direct interaction approximation (LDIA) by Kida & Goto (1997). These developments are crucial steps in extending the application area of the DIA-type closures to more realistic, inhomogeneous and anisotropic turbulent flows.

Then what is the role of FRR in these DIAs in Eulerian and Lagrangian coordinates? In Kraichnan's Eulerian DIA and LHDIA, no FRR was used upon solving the closed integro-differential equations for the correlation function and the linear response function. Instead, the FRR was invoked to justify the DIA: his Eulerian DIA and Lagrangian-history DIA were shown to be compatible to the FDT when it is applied to the energy-equipartitioned state (fully thermalised state) of the Galerkin truncated Euler equations, see e.g. Kraichnan (1964*a*), Kraichnan (1965) and Kraichnan (1966). By contrast, in the LRA and the LDIA, the integro-differential equation for the linear response function becomes identical to that of the correlation function. In other words, the FDT was obtained as a consequence of the closure approximations and hence used in solving the integro-differential equations.

These closures suggest that, whether or not the FDT holds, or whether a more general FRR should replace the FDT, depends on the coordinates (Eulerian or Lagrangian). We study this point by using DNS both in the Eulerian and Lagrangian (history) coordinates. As we mentioned in the previous subsection, to explore possible forms of FRR, we use two known FRRs for the randomly forced cases by Harada & Sasa (2005, 2006) and by Novikov (1965) and Carini & Quadrio (2010).

Finally, we comment on why studies about the linear response function in experiments or numerical simulations have not been common. One reason could be a technical one: a long-time average between the difference of the two nearby solutions is required in order to have a statistically converged result. Another one may be a conceptual one: some regard the linear response function itself as a somewhat abstract theoretical entity, leading to no interesting insights. Nevertheless, there are studies of the linear response function of the velocity Fourier modes in Eulerian coordinates, which include a case for homogeneous and isotropic turbulence (Carini & Quadrio 2010) and a case for turbulent channel flow in the context of turbulence control, see e.g. Luchini, Quadrio & Zuccher (2006) and references therein. In Lagrangian coordinates, the correlation function of the Lagrangian velocity Fourier modes has not been experimentally or numerically studied much either. The notable early numerical studies of the Lagrangian correlation functions include: Kaneda & Gotoh (1991) in two dimensions; Gotoh *et al.* (1993) for the Lagrangian-history velocity in three dimensions; Yeung & Pope (1989) and Kaneda, Ishihara & Gotoh (1999) in three dimensions for the Lagrangian velocity whose measuring time evolves forward in time.

The organisation of the paper is as follows. In the next two sections, we study the correlation function and the linear response function of the Fourier coefficients of the velocity in both Eulerian coordinates (§ 2) and Lagrangian coordinates (§ 3) via a DNS with a moderate Taylor-scale Reynolds number, $R_\lambda = 210$. The Reynolds number stays rather moderate since, for our purposes, integration over hundreds of large-scale eddy turnover times is required.

More specifically, in § 2 for the Eulerian coordinates, we discuss two FRRs which were the results of the randomly forced case obtained in Novikov (1965) and Carini & Quadrio (2010) and in our previous work (Matsumoto *et al.* 2014). The latter was obtained theoretically by adopting the relation in non-equilibrium statistical mechanics proposed by Harada & Sasa (2005, 2006). We numerically compare the two FRR expressions with a small random forcing with the linear response function measured without the random forcing, that is, in the deterministic case (§ 2.3).

In § 3 for the Lagrangian coordinates, by using the numerical method used in Kaneda & Gotoh (1991) and Gotoh *et al.* (1993), known as the passive vector method, we calculate the Lagrangian correlation and linear response functions, which are the same correlation and response functions as those considered in the abridged LHDIA (ALHDIA) by Kraichnan (1965, 1966). In both coordinates, the linear response function is directly calculated by using the numerical method proposed in Biferale *et al.* (2001). We derive the FRRs for the Eulerian coordinates in Appendix A and for the Lagrangian coordinates in Appendix B, but the Lagrangian FRRs are not numerically studied since their forms are not amenable to numerical simulations.

In § 4, we demonstrate numerically that the characteristic times associated with the Eulerian correlation and response functions have indeed the sweeping scaling, k^{-1} and that characteristic times associated with the Lagrangian ones have the Kolmogorov scaling, $k^{-2/3}$, in the inertial range.

In § 5 we present the discussion, which is followed by the concluding remarks in § 6. To show a possible use of the Novikov–Carini–Quadrio FRR, we describe attempts to theoretically estimate the time scales of the response functions at short times both in Eulerian and Lagrangian coordinates, which are in Appendices C and D.

2. Correlation and linear response functions in Eulerian coordinates

2.1. *Direct numerical simulation*

We first describe the method of our DNS. We consider the incompressible Navier–Stokes equations in a periodic cube with the side length 2π

$$\partial_t \boldsymbol{u} + (\boldsymbol{u} \cdot \nabla)\boldsymbol{u} = -\nabla p + \nu \nabla^2 \boldsymbol{u} + \boldsymbol{F}, \quad \nabla \cdot \boldsymbol{u} = 0, \tag{2.1}$$

where $\boldsymbol{u}$, p and ν denote the velocity, the pressure and the kinematic viscosity. The fluid density is normalised to unity. The velocity and the pressure are functions of the spatial coordinates $\boldsymbol{x}$ and the time t.

We add a large-scale forcing, $\boldsymbol{F}$, to keep the system in a statistically steady state, which is expressed in the Fourier space as

$$\hat{\boldsymbol{F}}(\boldsymbol{k}, t) = \begin{cases} \dfrac{\epsilon_{in}}{E_f} \hat{\boldsymbol{u}}(\boldsymbol{k}, t), & (0 < |\boldsymbol{k}| \le k_f), \\ \boldsymbol{0}, & (\text{otherwise}). \end{cases} \tag{2.2}$$

Here, $\hat{F}(k, t)$ and $\hat{u}(k, t)$ are the Fourier modes of the forcing and of the velocity, and k denotes the wavevector. The forcing parameters, ϵ_{in} and k_f, are the energy input rate and the maximum forcing wavenumber, respectively. By E_f, we denote the kinetic energy in the forcing range

$$E_f = \sum_{\substack{k \\ |k| \leq k_f}} \tfrac{1}{2} |\hat{u}(k, t)|^2. \tag{2.3}$$

With this setting, the numerically realised energy input rate by the forcing is indeed kept constant in time. This type of forcing is often used in DNSs by various authors, including Carini & Quadrio (2010).

Numerically, we solve the forced Navier–Stokes equations in the form of the vorticity equations with the Fourier-spectral method with N^3 grid points in the cube. We mainly set $N = 512$. The aliasing error is removed by the phase shift and the isotropic truncation (setting to zero the modes in $|k| \geq \sqrt{2}N/3$). We use the fourth-order Runge–Kutta scheme for the time stepping. We set the parameter values as follows: $\nu = 5.30 \times 10^{-4}$, $\epsilon_{in} = 1.00 \times 10^{-1}$, $k_f = 2.50$ and the size of the time step $\Delta t = 1.87 \times 10^{-3}$. We make ten random initial velocity fields with the energy spectrum $E(k) \propto k^4 \exp(-k^2/2)$ by setting identically and independently distributed Gaussian random variables to the real and imaginary parts of the incompressible velocity Fourier modes. The kinetic energy of the initial field is set to 0.50. For each initial data set, we run the simulation for ten large-scale turnover times and the statistics are collected after that. The resultant velocity fields are regarded as being in a statistically steady state with the Taylor-scale based Reynolds number being $R_\lambda = 210$. The large-scale eddy turnover time is $\tau_{to} = \langle L(t) \rangle / (2\langle E(t) \rangle/3)^{1/2} = 1.80$, which is calculated with the energy, $E(t) = \sum_k |\hat{u}(k, t)|^2/2$, and the integral-length scale, $L(t) = (3\pi)/(4E(t)) \times \sum_k |\hat{u}(k, t)|^2/|k|$. Here, $\langle \cdot \rangle$ denotes the average over time and the ensemble. The root-mean-square velocity is $u_{rms} = (2\langle E(t) \rangle/3)^{1/2} = 6.25 \times 10^{-1}$. The relation between the truncation wavenumber, $k_{max} = \sqrt{2}N/3$, and the Kolmogorov dissipation length scale, $\eta = (\nu^3/\langle \epsilon \rangle)^{1/4}$, is $k_{max}\eta = 1.51$. Here, $\langle \epsilon \rangle$ is the mean energy dissipation rate, which is here indeed equal to the prescribed energy input rate ϵ_{in}.

2.2. *Eulerian correlation and response function*

Here, we start with a decomposition of the incompressible velocity Fourier modes in Eulerian coordinates, which have only two independent components. Such a decomposition becomes crucially important when we later consider the FRRs by adding random noise to the Navier–Stokes equations. We adopt the Craya–Herring decomposition defined with the reference vector chosen here as $-e_z = (0, 0, -1)$, (see, e.g. Sagaut & Cambon 2008), which is

$$\hat{u}(k, t) = \hat{u}_\varphi(k, t)e_\varphi + \hat{u}_\theta(k, t)e_\theta. \tag{2.4}$$

Here, the unit vectors are written in the spherical coordinate system as $e_\varphi = (-\sin\varphi, \cos\varphi, 0)$ and $e_\theta = (\cos\theta\cos\varphi, \cos\theta\sin\varphi, -\sin\theta)$ with the polar angle θ $(0 \leq \theta \leq \pi)$ and the azimuthal angle φ $(0 \leq \varphi < 2\pi)$ of the wavevector $k = k(\sin\theta\cos\varphi, \sin\theta\sin\varphi, \cos\theta)$, where $k = |k|$. If k is aligned with the z-axis ($\theta = 0$ or π), we set $\varphi = 0$.

With this decomposition we define the correlation function of the velocity Fourier modes in the Eulerian coordinates as

$$C_{\alpha\beta}(\boldsymbol{k}, t \mid \boldsymbol{q}, s) = \langle \hat{u}_\alpha(\boldsymbol{k}, t)\hat{u}_\beta(\boldsymbol{q}, s)\rangle, \qquad (2.5)$$

where the indices, α, β, are either φ or θ.

In the numerical simulation, we calculate the shell average of the diagonal correlation functions

$$C_{\alpha\alpha}(k, t - s) = \frac{1}{N(k, k + \Delta k)} \sum_{\substack{\boldsymbol{k} \\ k \le |\boldsymbol{k}| < k + \Delta k}} C_{\alpha\alpha}(\boldsymbol{k}, t \mid -\boldsymbol{k}, s), \qquad (2.6)$$

where $N(k, k + \Delta k)$ is the number of Fourier modes lying in the annulus $k \le |\boldsymbol{k}| < k + \Delta k$. We set here $\Delta k = 1$. Notice that we assume isotropy in the Fourier space and a statistically steady state. We calculate the autocorrelation function of each mode, $C_{\alpha\alpha}(\boldsymbol{k}, t \mid -\boldsymbol{k}, s)$, by way of the temporal Fourier modes using the Wiener–Khinchin theorem. In practice, we record the time series of the real and imaginary parts of each Fourier mode and calculate the mean of the squared modulus of the Fourier transform of the time series.

Now we define the mean linear response function of the velocity Fourier modes in Eulerian coordinates as

$$G_{\alpha\beta}(\boldsymbol{k}, t \mid \boldsymbol{q}, s) = \left\langle \frac{\delta \hat{u}_\alpha(\boldsymbol{k}, t)}{\delta \hat{u}_\beta(\boldsymbol{q}, s)} \right\rangle. \qquad (2.7)$$

In our numerical calculation of the mean linear response function, we adopt the method used for the shell model in Biferale *et al.* (2001). Specifically, we take the numerical solution at time t_0 in the statistically steady state and consider two solutions: one starts from $\hat{u}_\alpha(\boldsymbol{q}, t_0)$ and the other starts from a perturbed solution, $\hat{u}_\alpha(\boldsymbol{q}, t_0) + \Delta\hat{u}_\alpha(\boldsymbol{q}, t_0)$. We then integrate the Navier–Stokes equations starting from the two initial conditions independently. At some later time $t \, (> t_0)$, the difference between the two solutions, which is denoted by $\Delta\hat{u}_\alpha(\boldsymbol{k}, t)$, yields one sample of the linear response function

$$G_{\alpha\beta}(\boldsymbol{k}, t \mid \boldsymbol{q}, t_0) \sim \frac{\Delta\hat{u}_\alpha(\boldsymbol{k}, t)}{\Delta\hat{u}_\beta(\boldsymbol{q}, t_0)}, \qquad (2.8)$$

provided that the difference stays so small that the evolution is essentially linear. We then take the average of the right-hand side of (2.8) over time t_0 and over the ensemble of several numerical solutions.

As in the correlation function, we calculate the shell average of the diagonal part of the response function,

$$G_{\alpha\alpha}(k, t - t_0) = \frac{1}{N(k, k + \Delta k)} \sum_{\substack{\boldsymbol{k} \\ k \le |\boldsymbol{k}| < k + \Delta k}} G_{\alpha\alpha}(\boldsymbol{k}, t \mid -\boldsymbol{k}, t_0). \qquad (2.9)$$

In the calculation of the shell average, we add the initial perturbation at time t_0 (the denominator in (2.8)) to all the modes in the shell. For the initial perturbation, we set only the real part: in other words, $\mathrm{Im}[\Delta\hat{u}_\alpha(-\boldsymbol{k}, t_0)] = 0$. We set the initial perturbation, $\mathrm{Re}[\Delta\hat{u}_\alpha(-\boldsymbol{k}, t_0)]$, to five per cent of the standard deviation of $|\hat{u}_\alpha(\boldsymbol{k}, t)|$ (the sign of the initial perturbation is always positive). We check that the shell-averaged response function calculated in this manner agrees well with the mode-wise response function, $G_{\alpha\alpha}(\boldsymbol{k}, t \mid -\boldsymbol{k}, t_0)$, which is calculated by adding the initial perturbation only to two modes $\hat{u}(\pm\boldsymbol{k}, t_0)$ with $\boldsymbol{k}$ and $-\boldsymbol{k}$ being within the same shell.
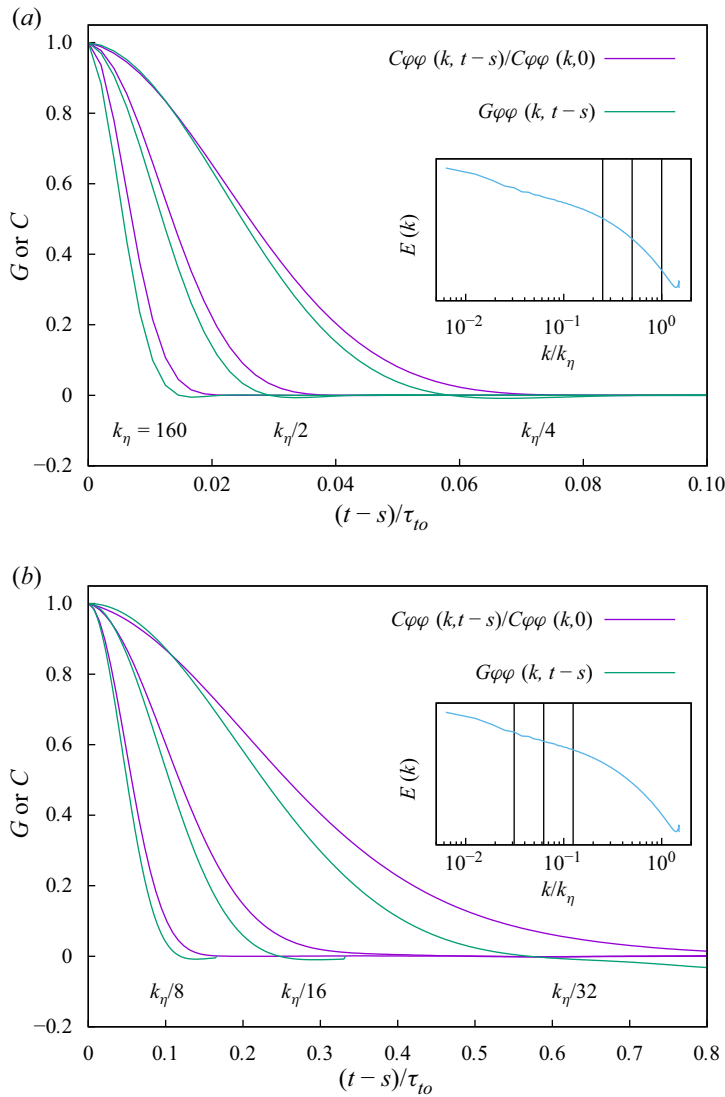
Figure 1. The shell-averaged correlation function and the shell-averaged mean linear response function of the diagonal φ-component for $k = k_\eta$, $k_\eta/2$, $k_\eta/4$ (*a*) and $k = k_\eta/8$, $k_\eta/16$, $k_\eta/32$ (*b*). Notice that the correlation function is normalised with the equal-time value $C_{\varphi\varphi}(k, 0)$. Here the large-scale eddy turnover time is $\tau_{to} = 1.80$. Insets: the averaged energy spectrum with the representative wavenumbers depicted by vertical lines.

In figure 1, we show the shell-averaged correlation functions normalised with the equal-time values and the shell-averaged linear response functions for six representative wavenumbers. The wavenumbers are chosen as powers of one half times the Kolmogorov dissipation wavenumber, $k_\eta = (\langle\epsilon\rangle/\nu^3)^{1/4} = 160$, up to the one in the energy-containing range, $k = k_\eta 2^{-5} = 2k_f = 5$. In figure 1 we show only the real parts of the correlation and response functions since the imaginary parts are approximately two orders of magnitude smaller than the real parts. For the shell-averaged other components, the correlation function $C_{\theta\theta}(k, t - s)$ is nearly identical to $C_{\varphi\varphi}(k, t - s)$ and the response function $G_{\theta\theta}(k, t - s)$ is nearly identical to $G_{\varphi\varphi}(k, t - s)$.
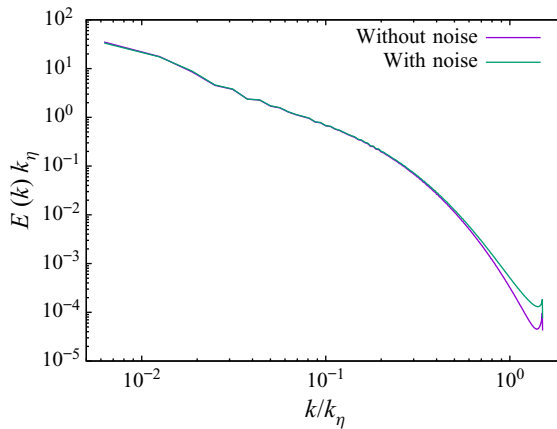
919 A9-8

Figure 2. Comparison of energy spectra with and without the small random forcing, $\hat{\boldsymbol{\xi}}(\boldsymbol{k}, t)$. Here, the noise variance parameters in (2.12) are $T = 10^{-6}$ and $\sigma(k) = k^{-1}$.

We here observe a small but measurable difference between the correlation function and the linear response function. In particular, the FDT, $C_{\varphi\varphi} \propto G_{\varphi\varphi}$, is invalid for all the representative wavenumbers spanning from the inertial range to the dissipation range. Here, we regard $k_f < k \leq k_\eta/4 = 40$ as the inertial range and $k > 40$ as the dissipation range based on the shape of the energy spectrum shown in the inset of figure 1. Another observation in figure 1 is the tendency that the response functions are generally smaller than the normalised correlation functions. We do not have an explanation of this tendency.

This breakdown of the FDT, which is as expected, is a manifestation of the fact that the velocity Fourier modes of turbulence are not described with the equilibrium statistical mechanics (Marconi *et al.* 2008) regardless of the wavenumber ranges. Here, we point out an apparently contradictory fact: the probability density functions (p.d.f.s) of the real and imaginary parts of the velocity Fourier modes in all the wavenumber ranges are known to become closer to the Gaussian distribution as we increase the Reynolds number (Brun & Pumir 2001). In our simulation, the p.d.f.s are indeed close to Gaussian for all the six wavenumbers selected in figure 1. Those p.d.f.s are shown in Appendix E. The Gaussian distribution implies the FDT, provided that there is no correlation among different wavenumber modes. An example with correlated degrees of freedom, whose marginal p.d.f. is near Gaussian, is carefully examined by Marconi *et al.* (2008). Indeed, they showed that the example does not satisfy the FDT. The homogeneous isotropic turbulence is another example of having a Gaussian (marginal) p.d.f. not showing the FDT.

Coming back to figure 1, despite the difference between the correlation function and the linear response function, we observe that their characteristic times defined, for example, as the integral time scales, seem to be of the same order of magnitude. This point will be studied in §4 together with the Lagrangian counterparts.

We end this section by commenting on details of the averaging of the correlation and response functions. We set the length of the temporal window for the correlation function to $1.85\tau_{to}$ for the small wavenumbers, $k = k_\eta/32, k_\eta/16$ and $k_\eta/8$, and to $0.265\tau_{to}$ for large wavenumbers, $k = k_\eta/4, k_\eta/2$ and k_η. The correlation functions shown in figure 1 are given in one half of these window lengths. We take a total of 15 such windows (5 windows in 3 simulations) in the averaging for the former set of k values and total 200 windows (20 windows in 10 simulations) for the latter set of k values. For the linear response function, the length of the temporal window for each wavenumber is $0.833\tau_{to}, 0.331\tau_{to}, 0.164\tau_{to}$

for the set of the small wavenumbers and $0.331\tau_{to}$ for the set of the large wavenumbers. The total number of windows are 20 (20 windows in 1 simulation), 100 (50 windows in 2 simulations) and 200 (100 windows in 2 simulations) respectively for the former set of three k values and 50 windows (50 windows in 1 simulation) for the latter set of three k values. Now the question with this sampling is whether the means of the correlation function and the linear response function shown in figure 1 are converged or not. To check this, we decrease the number of samples to $1/3$ and compare the averages over the full sample to those over the $1/3$ sample. The difference between the averages is at most a few per cent for both the correlation function and the response function. This is the case for large wavenumbers $k_\eta/16$ and $k_\eta/32$. For other wavenumbers, the difference between the samples is smaller than a few per cent. We regard the difference as small enough and consider that the average reached convergence. This difference in the averages is less than the discrepancy between the correlation function and the response functions shown in figure 1.

2.3. *FRR with random forcing*

As mentioned in § 1, the linear response function cannot be written in general with the two-point correlation function. However, if the uncorrelated Gaussian noise is added to the evolution equation, we can obtain several expressions of the linear response function (FRR) in terms of certain correlation functions. Here, we consider two FRRs and compare them with the linear response function without the noise shown in the previous subsection.

For homogeneous and isotropic Navier–Stokes turbulence, one of the expressions was derived by Novikov (1965) and numerically studied by Carini & Quadrio (2010). To give the precise expression, we now fix some notation. We first add the random Gaussian noise $\hat{\xi}_\alpha(\boldsymbol{k}, t)$ to the Navier–Stokes equations in Fourier space in addition to the large-scale forcing as

$$\partial_t \hat{u}_\alpha(\boldsymbol{k}, t) = (\boldsymbol{e}_\alpha)_j \left(-\frac{\mathrm{i}}{2}\right) P_{jlm}(\boldsymbol{k}) \sum_{\substack{\boldsymbol{p},\boldsymbol{q} \\ \boldsymbol{p}+\boldsymbol{q}+\boldsymbol{k}=\boldsymbol{0}}} \hat{u}_l(-\boldsymbol{p}, t)\hat{u}_m(-\boldsymbol{q}, t) - \nu k^2 \hat{u}_\alpha(\boldsymbol{k}, t)$$

$$+ \hat{F}_\alpha(\boldsymbol{k}, t) + \hat{\xi}_\alpha(\boldsymbol{k}, t). \tag{2.10}$$

Here, we take summation over the repeated indices j, l and m and the index α denotes the Craya–Herring component φ or θ. The projection operator is $P_{jlm}(\boldsymbol{k}) = k_m P_{jl}(\boldsymbol{k}) + k_l P_{jm}(\boldsymbol{k})$, where $P_{jl}(\boldsymbol{k}) = \delta_{jl} - k_j k_l/k^2$ with δ_{jl} being the Kronecker delta and $k = |\boldsymbol{k}|$. The real and imaginary parts of the noise, $\hat{\xi}_\alpha(\boldsymbol{k}, t)$, are identically and independently distributed Gaussian random variables with the following mean and covariance:

$$\langle \hat{\xi}_\alpha(\boldsymbol{k}, t) \rangle = 0, \tag{2.11}$$

$$\langle \hat{\xi}_\alpha(\boldsymbol{k}, t)\hat{\xi}_\beta(\boldsymbol{p}, s) \rangle = 2\sigma^2(k)T\delta_{\alpha,\beta}\delta_{\boldsymbol{k},-\boldsymbol{p}}\delta(t-s), \tag{2.12}$$

where $\sigma(k)$ is some function of k, T is a parameter which we call 'temperature' in this paper for convenience and $\delta(t)$ is the Dirac delta function.

The diagonal linear response function with the noise, denoted by $G_{\alpha\alpha}^{(T)}(\boldsymbol{k}, t \mid -\boldsymbol{k}, s)$, is expressed as

$$G_{\alpha\alpha}^{(T)}(\boldsymbol{k}, t \mid -\boldsymbol{k}, s) = \frac{1}{2\sigma^2(k)T}\left\langle \hat{u}_\alpha(\boldsymbol{k}, t)\hat{\xi}_\alpha(-\boldsymbol{k}, s) \right\rangle. \tag{2.13}$$

We denote the right-hand side of (2.13) as $J_{\alpha\alpha}^{(T)}(\boldsymbol{k}, t \mid -\boldsymbol{k}, s)$. This is the first FRR which we consider. The value of $J_{\alpha\alpha}^{(T)}(\boldsymbol{k}, t \mid -\boldsymbol{k}, s)$ at the equal time, $t - s = 0$, should be one, which is guaranteed by the variance (2.12). In Carini & Quadrio (2010), the expression (2.13) was shown numerically to be equal to the linear response function in the dissipation range without the random noise if the noise is sufficiently small.

This FRR holds in general for a randomly forced system. As the name, FRR, indicates, it gives the relation between the fluctuation (the random noise) and the response. The FRR (2.13) has been used in statistical mechanics, see for example Cugliandolo, Kurchan & Parisi (1994), and can be obtained also from the statistical field-theoretic formalism on the linear response function, see e.g. § 10.4 of Cardy (1996) or chapter 36 of Zinn-Justin (2002). The theoretical basis of Carini & Quadrio (2010) is Luchini *et al.* (2006), in which the FRR was referred to as a well-known result of signal theory. According to Marconi *et al.* (2008), this FRR, not only for the Navier–Stokes equations but also for general Langevin equations, is ascribed to Novikov (1965). In this paper we call it Novikov–Carini–Quadrio FRR.

Now we move to another expression of the linear response function in terms of the two-point or multi-point correlation functions of $\hat{u}$, which was outlined in Matsumoto *et al.* (2014). For brevity, we write the nonlinear term and the large-scale forcing as

$$\Lambda_\alpha(\boldsymbol{k}, t) = (e_\alpha)_j \left(-\frac{\mathrm{i}}{2}\right) P_{jlm}(\boldsymbol{k}) \sum_{\substack{\boldsymbol{p}, \boldsymbol{q} \\ \boldsymbol{p}+\boldsymbol{q}+\boldsymbol{k}=\boldsymbol{0}}} \hat{u}_l(-\boldsymbol{p}, t)\hat{u}_m(-\boldsymbol{q}, t) + \hat{F}_\alpha(\boldsymbol{k}, t). \qquad (2.14)$$

Using this $\Lambda_\alpha(\boldsymbol{k}, t)$, we have another expression of the diagonal response function as

$$G_{\alpha\alpha}^{(T)}(\boldsymbol{k}, t \mid -\boldsymbol{k}, s) = \frac{1}{2\sigma^2(k)T}\Big[2\nu k^2 C_{\alpha\alpha}(\boldsymbol{k}, t \mid -\boldsymbol{k}, s) - \big\{\langle\Lambda_\alpha^*(\boldsymbol{k}, t)\hat{u}_\alpha(\boldsymbol{k}, s)\rangle$$
$$+ \langle\Lambda_\alpha^*(\boldsymbol{k}, s)\hat{u}_\alpha(\boldsymbol{k}, t)\rangle\big\}\Big]. \qquad (2.15)$$

We denote the right-hand side of (2.15) as $H_{\alpha\alpha}^{(T)}(\boldsymbol{k}, t \mid -\boldsymbol{k}, s)$. This form was derived by adapting the Harada–Sasa relation of the nonlinear Langevin equation in non-equilibrium steady state (Harada & Sasa 2005, 2006) to the Navier–Stokes equations with Gaussian noise (2.10). We call $H_{\alpha\alpha}^{(T)}(\boldsymbol{k}, t \mid -\boldsymbol{k}, s)$ the Harada–Sasa FRR in this paper. Heuristically, the Harada–Sasa FRR can be also obtained from (2.13) by re-writing the noise $\hat{\xi}_\alpha(-\boldsymbol{k}, s)$ with the dissipation term, $\Lambda_\alpha(\boldsymbol{k}, t)$ and the time-derivative term via (2.10). We can next eliminate the time-derivative term by using the causality of the response function and the symmetry of the auto-correlation function $C_{\alpha\alpha}(\boldsymbol{k}, t \mid -\boldsymbol{k}, s)$. Then, we arrive at the Harada–Sasa FRR from the Novikov–Carini–Quadrio FRR. However, the original derivation of the Harada–Sasa FRR does not depend on (2.13). A derivation of (2.15) is given in Appendix A.

Now let us observe the structure of the Harada–Sasa FRR (2.15) at the formal level. It provides a closed expression of the linear response function in terms of the second-order correlation function and many third-order correlation functions (recall that $\Lambda_\alpha(\boldsymbol{k}, t)$ involves the nonlinear term as given in (2.14)). In particular, the second and third terms of the FRR (2.15) describe the deviation from the FDT, $G_{\alpha\alpha} \propto C_{\alpha\alpha}$, implying that the nonlinearity is responsible for the deviation. This point will be examined later numerically. Another observation concerns the value of $H_{\alpha\alpha}^{(T)}(\boldsymbol{k}, t \mid -\boldsymbol{k}, s)$ at the equal time, $t - s = 0$, which should be one. This is guaranteed by the statistical steadiness of the energy of each component of the Fourier mode, i.e. $\partial_t \langle|\hat{u}_\alpha(\boldsymbol{k}, t)|^2\rangle = 0$. More precisely, under the

steadiness, the numerator on the right-hand side of (2.15) at $t = s$ is equal to the energy input by the noise, $2\sigma^2 T$.

The two FRRs, which are basically equivalent expressions, hold owing to the random noise. However, the noise's role in this study is not physical but just theoretical, as mentioned in § 1. Let us argue that the two FRRs are consistent with the FDT in the absolute equilibrium where the velocity Fourier modes follow the Gaussian distribution and become independent from each other. For the Harada–Sasa FRR, the triple correlation vanishes in the absolute equilibrium and hence it becomes consistent with the FDT. For the Novikov–Carini–Quadrio FRR, we consider it in the following manner. First, the absolute equilibrium for this case can be realised by the Langevin noise with a finite T and $\sigma(k) = k^1$, as found by Forster, Nelson & Stephen (1977). Second, let us here ignore the large-scale forcing $\hat{\boldsymbol{F}}(\boldsymbol{k}, t)$ for the sake of the argument. In this setting, the Navier–Stokes equations become just an Ornstein–Uhlenbeck process given by the viscous term and the noise. Then we can see that the Novikov–Carini–Quadrio FRR expression is consistent with the FDT.

Now, a question we numerically address is the same as Carini & Quadrio (2010): whether the FRRs with a sufficiently small noise amplitude T are good approximations of the response function without the noise. To answer this question, we compare the shell-averaged Novikov–Carini–Quadrio FRR, $J_{\alpha\alpha}^{(T)}(\boldsymbol{k}, t \mid -\boldsymbol{k}, s)$, and the Harada–Sasa FRR, $H_{\alpha\alpha}^{(T)}(\boldsymbol{k}, t \mid -\boldsymbol{k}, s)$, with a small T to the response function without the noise, $G_{\alpha\alpha}(k \mid t - s)$. The shell averages of the FRRs are defined in a similar fashion to (2.9). As a small amplitude, we here take the value of the temperature $T = 10^{-6}$ and $\sigma(k) = k^{-1}$ (which corresponds to the wavenumber-independent noise spectrum). With this choice, the energy spectrum is close to that of the noiseless case except for the far dissipation range as shown in figure 2. To calculate the FRRs, we solve the stochastic Navier–Stokes equations in terms of the vorticity equations in the Cartesian xyz components with the same fourth-order Runge–Kutta method as in the deterministic case (we do not use a stochastic scheme). The noise is generated in the Craya–Herring components, $(\hat{\xi}_\varphi(\boldsymbol{k}, t), \hat{\xi}_\theta(\boldsymbol{k}, t))$, and then transformed to the xyz components. This noise is added for all the wavenumbers in the computational (Cartesian) Fourier domain. The time-step size is $\Delta t = 1.87 \times 10^{-3}$, which is the same as in the deterministic case. In the Runge–Kutta scheme, we do not generate the random noise at the middle time $t + \Delta t/2$ but use the same noise generated at the time t.

The numerical calculations of the two FRRs are done as follows. We show here only the φ component ($\alpha = \varphi$). For $J_{\varphi\varphi}^{(T)}(\boldsymbol{k}, t \mid -\boldsymbol{k}, s)$, we use the same method as Carini & Quadrio (2010), namely, calculate the correlation between $\hat{u}_\varphi(\boldsymbol{k}, t)$ and $\hat{\xi}_\varphi(-\boldsymbol{k}, s)$. The calculation of $H_{\varphi\varphi}^{(T)}(\boldsymbol{k}, t \mid -\boldsymbol{k}, s)$ is done by computing the correlations involved, such as $\Lambda_\varphi^*(\boldsymbol{k}, t)$ and $\hat{u}_\varphi(\boldsymbol{k}, s)$ and so forth. The results are shown in figure 3. We observe that the three response functions agree well for large wavenumbers, more precisely, from the end of the inertial range to the dissipation wavenumber k_η. For smaller wavenumbers, the two expressions start to deviate from each other. While the Novikov–Carini–Quadrio expression $J^{(T)}$ keeps a better agreement with G, the Harada–Sasa expression $H^{(T)}$ shows sizeable deviations. By increasing the number of samples, the deviations becomes smaller, however. The worse agreement of $H^{(T)}$ has been anticipated from our previous study of the shell model (Matsumoto *et al.* 2014) since the summations in the shell-model equivalent of (2.15) caused loss of significant digits, in particular, in the inertial range. This is also the case for the Navier–Stokes case, as we will now show. The Novikov–Carini–Quadrio FRR, $J^{(T)}$, does not have such a cancellation and hence exhibits better agreement.
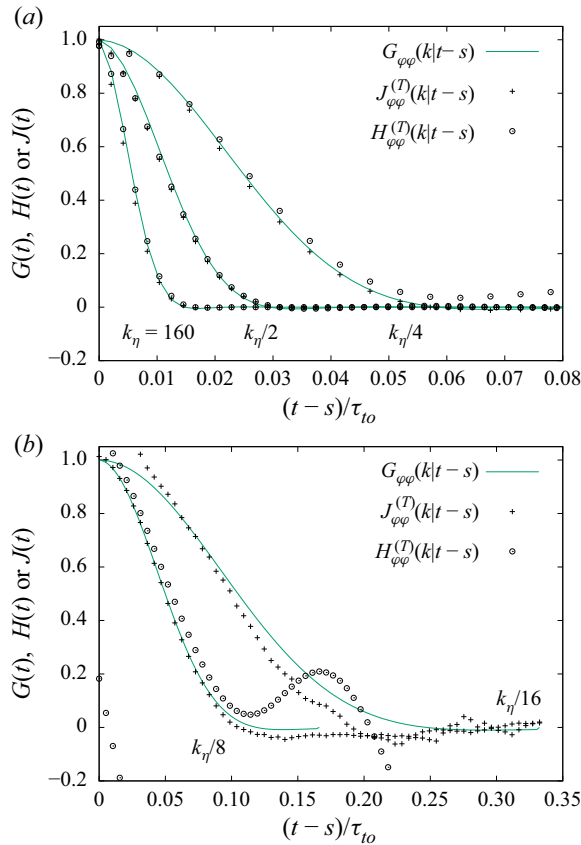
Figure 3. The shell-averaged Novikov–Carini–Quadrio expression of the linear response function, $J^{(T)}$ $(k, t - s)$, the Harada–Sasa expression, $H^{(T)}(k, t - s)$, and the linear response function in the noiseless case, $G(k, t - s)$, which is the same as shown in figure 1. Here, the noise is specified by $\sigma(k) = k^{-1}$ and $T = 10^{-6}$; (a) for $k = k_\eta, k_\eta/2, k_\eta/4$, (b) for $k = k_\eta/8, k_\eta/16$. The Harada–Sasa expression $H^{(T)}$ for $k = k_\eta/16$ (plotted with circles) has the numerical value of 0.2 at the origin and becomes negative for $(t - s)/\tau_{to} > 0.03$, implying that statistical convergence is not reached. Here, the $k = k_\eta/32 = 5$ case is not shown because of similar but much larger discrepancies.

To discuss the cancellation of significant digits in (2.15), we write separately the shell averages of the nonlinear and linear parts of the Harada–Sasa FRR as

$$L_\alpha(k, t, s) = \frac{1}{N(k, k + \Delta k)} \sum_{\substack{\boldsymbol{k} \\ k \leq |\boldsymbol{k}| < k + \Delta k}} \frac{1}{2\sigma^2(k)T} \langle \Lambda_\alpha^*(\boldsymbol{k}, t)\hat{u}_\alpha(\boldsymbol{k}, s) \rangle, \qquad (2.16)$$

$$D_\alpha(k, t, s) = \frac{1}{N(k, k + \Delta k)} \sum_{\substack{\boldsymbol{k} \\ k \leq |\boldsymbol{k}| < k + \Delta k}} \frac{1}{\sigma^2(k)T} \nu k^2 C_{\alpha\alpha}(\boldsymbol{k}, t \mid -\boldsymbol{k}, s). \qquad (2.17)$$

Here, notice that the wavenumber factors, $\sigma(k)$ and k^2, are inside the summation. This is necessary for our limited range of the wavenumbers, $k_\eta/16 = 10 \leq k \leq 160 = k_\eta$ with $\Delta k = 1$. The shell-averaged Harada–Sasa FRR is given as $H_{\alpha\alpha}^{(T)}(k, t - s) = D_\alpha(k, t, s) - [L_\alpha(k, t, s) + L_\alpha(k, s, t)]$ (which is shown in figure 3). These shell-averaged parts are plotted in figure 4 for $k = k_\eta/4$ and $k_\eta/8$. Although the overall shapes of the triple
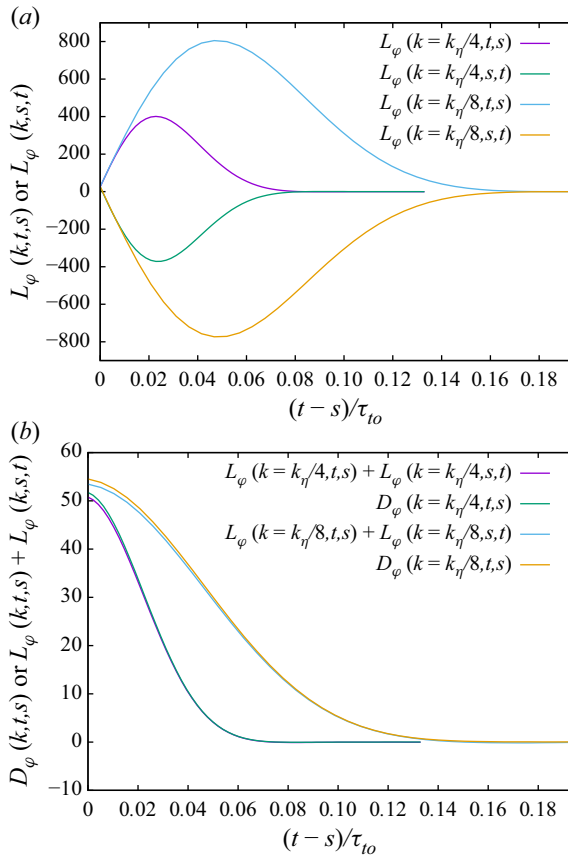
919 A9-13

Figure 4. Twofold cancellations involved in evaluation of the Harada–Sasa FRR,
$H^{(T)}_{\varphi\varphi}(k, t-s) = D_\varphi(k, t-s) - [L_\varphi(k, t, s) + L_\varphi(k, s, t)]$, with $R_\lambda = 210 (k_\eta = 160)$.

correlations $L_\varphi(k, t, s)$ and $L_\varphi(k, s, t)$ ($t > s$) are nearly symmetrical with respect to the horizontal axis, the former is slightly larger than the latter in magnitude. The positive sign of $L_\varphi(k, t, s)$ can be a reflection of the direct energy cascade. We can now see that the cancellation is twofold: the first is in the sum $L_\varphi(k, t, s) + L_\varphi(k, s, t)$ and the second is in the subtraction of the sum from the viscous term. Roughly one significant digit is lost in each cancellation. This implies that, in order to calculate $H^{(T)}$ with the right order of magnitude, the correlations involved should be calculated with more than 3-digit accuracy. This is a demanding numerical requirement in particular for those in small wavenumbers since a very long integration time is required to make fluctuation of the average small.

Next, we consider Reynolds number effect on the Harada–Sasa FRR. With a smaller Reynolds number, $R_\lambda = 130$ with $\nu = 1.34 \times 10^{-3}$, let us show the FRR in figure 5 and the cancellations in the Harada–Sasa FRR in figure 6. In these figures, the noise is specified by $\sigma(k) = k^{-1}$ and $T = 10^{-6}$. Comparing figure 5 to figure 3(a) for the higher Reynolds number, we find that the FRR's behaviour is similar, although the agreement for the largest k becomes poor for the lower Reynolds number case. We now argue that this poor agreement is due to the cancellations, which become more severe as we decrease the Reynolds number. As shown in figure 6, the twofold cancellations occur also for the lower Reynolds number case. Here, we notice in figure 6(b) that the values of D_φ and the sum of
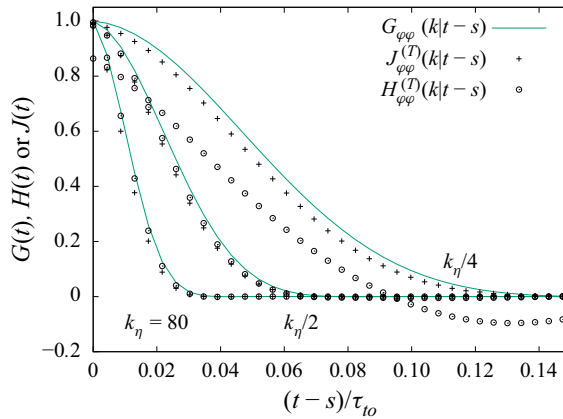
Figure 5. Same as figure 3 but with a lower Reynolds number $R_\lambda = 130$ ($k_\eta = 80$).

L_φ for $k = k_\eta/4 = 20$ around the origin ($t - s = 0$) with $R_\lambda = 130$ is approximately 100. In contrast, the corresponding value is 55 for $k = k_\eta/8 = 20$ with $R_\lambda = 210$, as shown in figure 4(*b*). If this value at the origin is smaller, then the second cancellation, namely the loss of significant digits, becomes less severe. This gives rise to the poor agreement for $k = k_\eta/4$ shown in figure 5. These observation suggest that, as we increase the Reynolds number, the Harada–Sasa FRR agrees better with the linear response function for small wavenumbers.

Now let us come back to the formal observation of the Harada–Sasa FRR (2.15). We previously noted that the sum of the second and third terms on the right-hand side of (2.15) is formally responsible for the deviation from the FDT. This formal observation assumes that the functional form of the sum as the time difference, $t - s$, is very much different from that of the first term in (2.15). However, this assumption is not valid, as indicated by the second cancellation. As shown in figure 4(*b*), the numerical data demonstrate that the functional form of the sum is quite close to that of the viscous contribution. Contrary to the formal observation of (2.15), in reality, the deviation from the FDT arises equally both from the viscous contribution and the nonlinear contributions. The viscous contribution to the deviation is not at all negligible for all of the time range. By contrast, in the shell-model study of the Harada–Sasa FRR (Matsumoto *et al.* 2014), the second cancellation was not observed. This is probably owing to the extremely small kinematic viscosity of the shell model. It is also consistent with our observation that the second cancellation for the Navier–Stokes case becomes less severe as we decrease the Reynolds number. It is then suggested that the second cancellation does not occur for the Navier–Stokes case if the Reynolds number is sufficiently large. There is one technical remark, however; when we increase the Reynolds number, we may need to adjust the noise temperature T to have the same energy spectrum with $T = 0$ as we illustrated in figure 2. Another implication of the second cancellation shown in figure 4(*b*) is that the sum of the triple correlations, $L_\varphi(k, t, s) + L_\varphi(k, s, t)$, is very close to $D_\varphi(k, t - s)$ which is the correlation function multiplied by νk^2 in the whole $t - s$ domain. This suggests that this combination of the triple correlations can be well approximated with the pair correlation with a suitable constant depending on k, which is considered to be a kind of eddy viscosity.

Regarding the wavenumber-dependent noise amplitude $\sigma(k)$, we have considered numerically so far only one case, $\sigma(k) = k^{-1}$ with $T = 10^{-6}$. In principle, the Novikov–Carini–Quadrio FRR and the Harada–Sasa FRR hold for any $\sigma(k)$ and T.
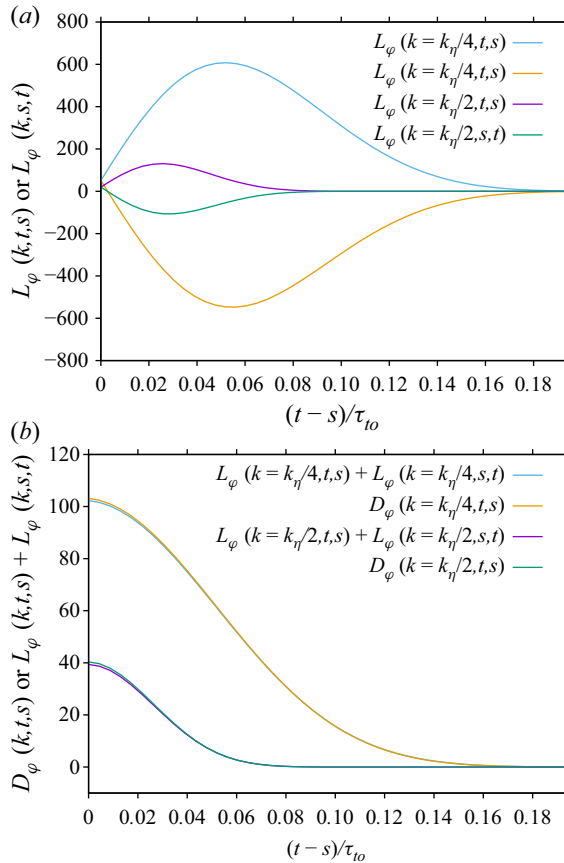
Figure 6. Same as figure 4 but with a lower Reynolds number $R_\lambda = 130$ ($k_\eta = 80$).

We now briefly mention that the FRRs hold numerically for other choices of $\sigma(k)$ and T. Indeed, with an arbitrary choice of $\sigma(k)$ and T, the corresponding numerical solution can be quite different from what we wish to simulate as turbulent flow in nature. For example, the energy spectrum may be different from the Kolmogorov spectrum $E(k) \propto k^{-5/3}$. But our focus here is to use those FRRs with the random noise to approximate the linear response function without the noise. For this purpose, given $\sigma(k)$, we expect that sufficiently small T enables us to have the Eulerian velocity with the noise being statistically close to the one without the noise. It should be noticed here that, in addition to the noise, we have the large-scale forcing $\hat{F}(k, t)$. As one variation of k-dependence of $\sigma(k)$, we set $\sigma(k) = k^{-2}$ with $R_\lambda = 130$. In this case, we find that $T = 10^{-4}$ is small enough to have the same $E(k)$ as in the noiseless case. The FRRs for this noise behave similarly to those as depicted in figure 3.

To test the FRRs for the velocity field with $E(k) \not\propto k^{-5/3}$, an easy way is to use a suitable $\sigma(k)$ and to increase the temperature T. In one numerical experiment with $R_\lambda = 130$, we consider $\sigma(k) = k^{-1}$ and $T = 10^{-4}$, where the energy spectrum becomes $E(k) \propto k^{-1}$ for all the wavenumbers (if T is much smaller than that value, $E(k)$ follows $k^{-5/3}$ because of the large-scale forcing $\hat{F}(k, t)$). This spectrum $E(k) \propto k^{-1}$ is consistent with the renormalisation group analysis for $\sigma(k) = k^{-1}$, see, e.g. Frisch (1996) and Sain, Manu & Pandit (1998). In this non-Kolmogorov case, the directly measured linear

919 A9-16

response function $G_{\varphi\varphi}^{(T)}$ also differs from the noiseless one $G_{\varphi\varphi}$. We here also find that the Novikov–Carini–Quadrio FRR and the Harada–Sasa FRR agree well with the directly measured response function $G_{\varphi\varphi}^{(T)}$. From these examples it is now clear that those FRRs are not limited to the case characterised by the Kolmogorov spectrum.

To summarise, we conclude that the two FRRs with the sufficiently small random noise agree well with the linear response function in the deterministic setting (without the random noise) at least from the dissipation range up to the middle of the inertial range. In practice, the Novikov–Carini–Quadrio FRR, $J^{(T)}$, is numerically easier to calculate accurately than the Harada–Sasa FRR, $H^{(T)}$. The direct evaluation of the linear response function (Biferale *et al.* 2001) yields the least fluctuating result among the three methods, although its computational cost is high. It requires us to solve simultaneously two solutions of the Navier–Stokes equations. In principle, one solution of the Navier–Stokes equations and one solution of the linearised Navier–Stokes equations are sufficient for the direct evaluation. However, its cost is not very different from solving the two fully nonlinear equations. We show a possible theoretical use of the Novikov–Carini–Quadrio FRR in Appendix C, which is related to the subject of § 4.

The details of the averaging of the FRRs in this section are as follows. With $R_\lambda = 210$, the length of the temporal window for calculating $H^{(T)}$ and $J^{(T)}$ is $0.267\tau_{to}$ for the large wavenumbers $k = k_\eta, k_\eta/2$ and $k_\eta/4$. The total number of the windows is 200. In one simulation we take 20 windows consecutively. Furthermore, we repeat this for the ensemble of 10 simulations. For the small wavenumbers, $k = k_\eta/8$ and $k_\eta/16$, the window length is $0.667\tau_{to}$. The total number of windows is 100, which consists of 10 consecutive windows in each simulation of the ensemble. In the low Reynolds number ($R_\lambda = 130$) case shown in figures 5 and 6, the time window to calculate the FRRs is $0.554\tau_{to}$ and the total number of windows is 200. We take 100 windows consecutively in one simulation. We repeat this for the ensemble of two simulations.

3. Correlation and linear response function in Lagrangian coordinates

In this section we numerically study the correlation function and the linear response function of the velocity Fourier coefficients in Lagrangian coordinates. To calculate them numerically with spectral accuracy, we employ the passive vector method proposed by Kaneda & Gotoh (1991). This leads to the linear response function with respect to the labelling time, not the measuring time of the Lagrangian velocity. Hence, the linear response function studied here is the one used in Kraichnan's ALHDIA (Kraichnan 1966). Our goal here is to measure the two functions in the deterministic setting reliably. This result will be used to extract time scales in the next section. Contrary to the previous section, we study only theoretically FRR expressions of the Lagrangian response function in Appendices B and D.

3.1. *Passive vector method for the Lagrangian velocity*

We use Kraichnan's notation of the Lagrangian velocity, $\boldsymbol{v}(\boldsymbol{a}, t_\ell \mid t_m)$, also known as the generalised velocity (Kraichnan 1965). This is the velocity of a fluid particle measured at time $t = t_m$, which is called the measuring time. This particular fluid particle passes the point whose coordinate is $\boldsymbol{a}$ at time $t = t_\ell$. The coordinate $\boldsymbol{a}$ and the time t_ℓ are called the Lagrangian label and the labelling time, respectively. An intuitively natural choice is $t_m \geq t_\ell$ as made in the LRA and the LDIA. In the ALHDIA the opposite choice $t_\ell \geq t_m$ was made: one lets the labelling time vary by keeping the measuring time constant. In this

case, the velocity measured at the fixed time, t_m, is a Lagrangian invariant later in the labelling time. Therefore, we have the following passive vector equations describing the labelling-time evolution of the Lagrangian velocity:

$$\partial_{t_\ell} \boldsymbol{v}(\boldsymbol{x}, t_\ell \mid t_m) + (\boldsymbol{u}(\boldsymbol{x}, t_\ell) \cdot \nabla)\boldsymbol{v}(\boldsymbol{x}, t_\ell \mid t_m) = \boldsymbol{0}. \quad (3.1)$$

The initial condition of the Lagrangian velocity is given by the Eulerian velocity at the measuring time.

In our numerical simulation of the statistically steady state, we set the initial Lagrangian velocity from the Eulerian velocity by $\boldsymbol{v}(\boldsymbol{x}, t_m \mid t_m) = \boldsymbol{u}(\boldsymbol{x}, t_m)$, we then solve the passive vector equation (3.1) and the Navier–Stokes equations (2.1) simultaneously with the same numerical method as described in § 2.1. After some long time, we reset the Lagrangian velocity to the current Eulerian velocity. Repeating this procedure, we obtain an ensemble of the Lagrangian velocity evolving in the labelling time.

It is known that this passive vector method for the Lagrangian velocity has a serious numerical difficulty due to the lack of any dissipation in (3.1), see e.g. Gotoh *et al.* (1993). The difficulty is that the energy spectrum of the Lagrangian velocity, $E_v(k, t_\ell)$, starting with the same spectrum as the Eulerian one at $t_\ell = t_m$, increases quickly, especially at high wavenumbers. Hence, the truncation error of the Lagrangian velocity becomes large in a finite time. The question is, how long we can trust the Lagrangian velocity calculated with the passive vector method for a given spatial resolution? We will examine this point in the next subsection.

3.2. *Lagrangian correlation and linear response function*

Having obtained the Fourier coefficient of the Lagrangian velocity, $\hat{\boldsymbol{v}}(\boldsymbol{k}, t_\ell \mid t_m)$, we consider the following Lagrangian correlation function:

$$C_{jn}^{(L)}(\boldsymbol{k}, \boldsymbol{q}, t_\ell \mid t_\ell, t_m) = \langle \hat{v}_j(\boldsymbol{k}, t_\ell \mid t_\ell)\hat{v}_n(\boldsymbol{q}, t_\ell \mid t_m) \rangle = \langle \hat{u}_j(\boldsymbol{k}, t_\ell)\hat{v}_n(\boldsymbol{q}, t_\ell \mid t_m) \rangle \quad (3.2)$$

and the linear response function

$$G_{jn}^{(L)}(\boldsymbol{k}, \boldsymbol{q}, t_\ell \mid t_\ell, t_m) = \left\langle \frac{\delta \hat{v}_j(\boldsymbol{k}, t_\ell \mid t_\ell)}{\delta \hat{v}_n(\boldsymbol{q}, t_\ell \mid t_m)} \right\rangle = \left\langle \frac{\delta \hat{u}_j(\boldsymbol{k}, t_\ell)}{\delta \hat{v}_n(\boldsymbol{q}, t_\ell \mid t_m)} \right\rangle, \quad (3.3)$$

for $t_\ell \geq t_m$. Notice that the two functions in this time ordering are the same as used in the ALHDIA. The indices, j and n, take values 1, 2 or 3 which correspond to the x, y and z components, respectively. The Lagrangian velocity ceases to be solenoidal for $t_\ell > t_m$. To define the linear response function in (3.3), we adopt the notation used by Kida & Goto (1997). Hence, the variation is with respect to the velocity, not the infinitesimal probe force or the source term.

Let us compare the Lagrangian response function (3.3) with those Lagrangian response functions used in the DIAs. The one used in the LHDIA (Kraichnan 1965) corresponds to

$$G_{jn}^{(L)}(\boldsymbol{k}, t_\ell \mid t_m; \boldsymbol{q}, s_\ell \mid s_m) = \left\langle \frac{\delta \hat{v}_j(\boldsymbol{k}, t_\ell \mid t_m)}{\delta \hat{f}_n(\boldsymbol{q}, s_\ell \mid s_m)} \right\rangle, \quad (3.4)$$

with $t_\ell \geq t_m$ and $s_\ell \geq s_m$. Hence, four time variables are involved in the LHDIA. Here, $\hat{\boldsymbol{f}}(\boldsymbol{q}, s_\ell \mid s_m)$ is the Fourier mode of the infinitesimal probe force added to the right-hand

919 A9-18

side of (3.1). Another one used in the ALHDIA (Kraichnan 1965, 1966) is an abridged version of (3.4),

$$G_{jn}^{(L)}(\boldsymbol{k}, t_\ell \mid t_\ell; \boldsymbol{q}, t_\ell \mid t_m) = \left\langle \frac{\delta \hat{v}_j(\boldsymbol{k}, t_\ell \mid t_\ell)}{\delta \hat{f}_n(\boldsymbol{q}, t_\ell \mid t_m)} \right\rangle, \tag{3.5}$$

where only two time variables are involved and the numerator is an equal-time velocity. This (3.5) coincides with (3.3), which we will study numerically. Yet another one used in the LRA and the LDIA is

$$G_{jn}^{(L)}(\boldsymbol{k}, t_\ell \mid t_m; \boldsymbol{q}, t_\ell \mid t_\ell) = \left\langle \frac{\delta \hat{v}_j(\boldsymbol{k}, t_\ell \mid t_m)}{\delta \hat{g}_n(\boldsymbol{q}, t_\ell \mid t_\ell)} \right\rangle, \tag{3.6}$$

with $t_\ell \leq t_m$ (Kaneda 1981; Kida & Goto 1997). This time ordering is different from that in the ALHDIA and our DNS study. Here, $\hat{\boldsymbol{g}}(\boldsymbol{q}, t_\ell \mid t_m)$ is the infinitesimal probe force added to the right-hand side of the measuring-time evolution equation of the Lagrangian velocity (B4): see also Appendices B and D.

We now move to DNS of (3.2) and (3.3). We calculate the correlation function (3.2) from the Lagrangian velocity in the same way as the Eulerian one. Let us here write the time of the Eulerian simulation as t. For the direct calculation of the response function (3.3), we add a small initial perturbation $\Delta \hat{\boldsymbol{u}}(\boldsymbol{k}, t_0)$ at $t = t_0$, to both the Eulerian and Lagrangian velocity fields. This 'initial' time t_0 for the perturbation becomes the measuring time for the Lagrangian velocity, namely, $t_0 = t_m$. We then consider evolution in the labelling time $t = t_\ell (\geq t_m)$ of the two pairs of velocity fields: the unperturbed pair, $(\hat{\boldsymbol{u}}(\boldsymbol{k}, t), \hat{\boldsymbol{v}}(\boldsymbol{k}, t \mid t_m))$, and the perturbed pair, $(\hat{\boldsymbol{u}}'(\boldsymbol{k}, t), \hat{\boldsymbol{v}}'(\boldsymbol{k}, t \mid t_m))$. For the two pairs, we solve the Navier–Stokes equations (2.1) and the passive vector equations (3.1) simultaneously. More specifically, the starting condition of the perturbed pair is $\hat{\boldsymbol{u}}'(\boldsymbol{k}, t_m) = \hat{\boldsymbol{u}}(\boldsymbol{k}, t_m) + \Delta \hat{\boldsymbol{u}}(\boldsymbol{k}, t_m)$ and $\hat{\boldsymbol{v}}'(\boldsymbol{k}, t_m \mid t_m) = \hat{\boldsymbol{u}}'(\boldsymbol{k}, t_m)$. For the unperturbed Lagrangian velocity, $\hat{\boldsymbol{v}}(\boldsymbol{k}, t_m \mid t_m) = \hat{\boldsymbol{u}}(\boldsymbol{k}, t_m)$. The response function at labelling time t can be obtained via $[\hat{\boldsymbol{u}}'(\boldsymbol{k}, t) - \hat{\boldsymbol{u}}(\boldsymbol{k}, t)]/[\hat{\boldsymbol{v}}'(\boldsymbol{k}, t \mid t_m) - \hat{\boldsymbol{v}}(\boldsymbol{k}, t \mid t_m)]$. We repeat this procedure to calculate the Lagrangian response function.

In figure 7, we show the shell-averaged correlation and response functions

$$C^{(L)}(k, t_\ell - t_m) = \frac{1}{3N(k, k + \Delta k)} \sum_{\substack{\boldsymbol{k} \\ k \leq |\boldsymbol{k}| < k + \Delta k}} C_{jj}^{(L)}(\boldsymbol{k}, -\boldsymbol{k}, t_\ell \mid t_\ell, t_m), \tag{3.7}$$

$$G^{(L)}(k, t_\ell - t_m) = \frac{1}{3N(k, k + \Delta k)} \sum_{\substack{\boldsymbol{k} \\ k \leq |\boldsymbol{k}| < k + \Delta k}} G_{jj}^{(L)}(\boldsymbol{k}, -\boldsymbol{k}, t_\ell \mid t_\ell, t_m). \tag{3.8}$$

Here, we take summation over the index j. We add the initial perturbation $\Delta \hat{u}_j(\boldsymbol{k}, t_m)$ for all the modes within the shell $k \leq |\boldsymbol{k}| < k + \Delta k$. The initial perturbation for each mode is set as $\Delta \hat{\boldsymbol{u}}(\boldsymbol{k}, t_m) = \Delta u_0 \boldsymbol{e}_\varphi + \Delta u_0 \boldsymbol{e}_\theta$. Here, Δu_0 is a real positive number whose magnitude is five per cent of the standard deviation of $|\hat{u}_\varphi(\boldsymbol{k}, t)|$.

Before discussing the results shown in figure 7, let us first consider the effect of the truncation error of the passive vector method. As shown in figure 7, it takes approximately one large-scale turnover time, which is approximately $\tau_{to} = 1.80$, for the correlation function to decrease to 20 % of the value at the origin $t_\ell - t_m = 0$ for the small wavenumber $k = k_\eta/16$. The question is then, with the resolution $k_{max}\eta = 1.50$, whether we can trust the computed correlation function and response function up to this time lag, $t_\ell - t_m \simeq \tau_{to}$. To answer this question, we do the following
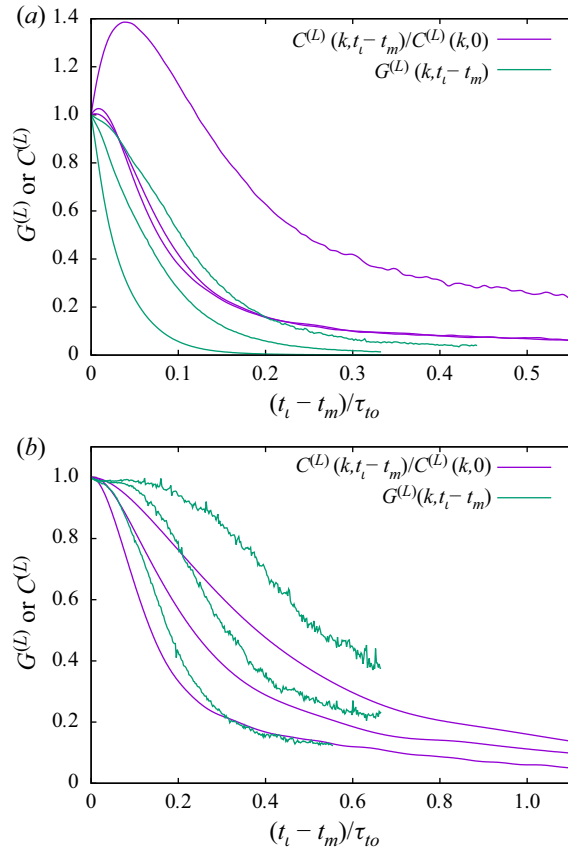
Figure 7. Shell-averaged correlation functions and linear response functions in Lagrangian coordinates for $k = k_\eta, k_\eta/2, k_\eta/4$ from left to right (*a*) and for $k = k_\eta/8, k_\eta/16, k_\eta/32$ from left to right (*b*). We show only the real parts since the imaginary parts are orders-of-magnitude smaller. The correlations of $k = k_\eta/2$ and $k_\eta/4$ are very close to each other. The increase of the correlation functions at short time is discussed in the text. The noisy behaviour of the response functions is due to lack of the statistical samples. In (*b*), the response functions are calculated up to around $t_\ell - t_m = 0.55\tau_{to}$.

resolution study. We decrease the Reynolds number to $R_\lambda = 130$ by setting the kinematic viscosity to $\nu = 1.34 \times 10^{-3}$. We compute this case with two resolutions, 256^3 and 512^3 grid points. The two simulations yield $k_{max}\eta = 1.50$ and 3.00, respectively. The large-scale turnover time is approximately 1.74. We compare the correlation functions calculated with the two resolutions in figure 8. We observe that the correlation functions agree well up to approximately one large-scale turnover time. Regarding the Lagrangian response function, whose numerical calculation is costly, we further decrease the Reynolds number to $R_\lambda = 70$ ($\nu = 3.75 \times 10^{-3}$) and calculate the solutions with two resolutions, 128^3 and 256^3 grid points. The two simulations have $k_{max}\eta = 1.63$ and 3.26. The large-scale turnover time is now 1.86. The comparison of the response function is shown in figure 9. We observe that the response functions for the small wavenumbers agree well up to one turnover time. Therefore, we infer that $k_{max}\eta = 1.50$ is sufficient to study the correlation function and the response function up to one large-scale turnover time in our study. In Gotoh *et al.* (1993), $k_{max}\eta = 2.0$ is recommended, however.

Having checked that the correlation function and the response function are reliable up to $t_\ell - t_m \simeq \tau_{to}$, we now list observations from figure 7. First, the Lagrangian
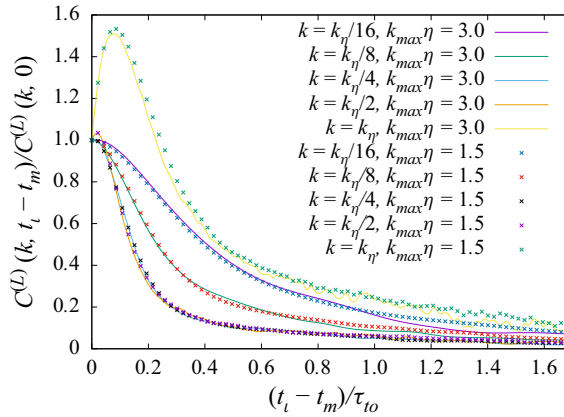
919 A9-20

Figure 8. Resolution dependence of the Lagrangian correlation function for $R_\lambda = 130$. The Kolmogorov dissipation wavenumber is $k_\eta = 80$. The truncation wavenumbers of the two resolutions are $k_{max} = 120$ and 241. The correlation functions of $k = k_\eta/4$ and $k_\eta/2$ are again very close, as in figure 7.
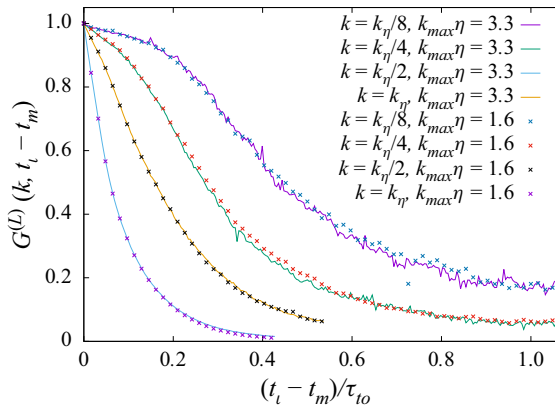

Figure 9. Resolution dependence of the Lagrangian linear response function for $R_\lambda = 70$. The Kolmogorov dissipation wavenumber is here $k_\eta = 37$ For simplicity, we take $k_\eta/2$, $k_\eta/4$ and $k_\eta/8$ as $k = 18, 9$ and 5, respectively. The truncation wavenumbers of the two resolutions are $k_{max} = 60$ and 120.

correlation functions decrease more slowly than the Eulerian ones, which will be analysed quantitatively in the next section. Second, the correlation functions at the equal time $t_\ell - t_m = 0$ have positive slopes (time derivatives) and hence their peaks are shifted from the origin for all the six wavenumbers shown in figure 7. For small wavenumbers, the slopes at the origin in figure 7 are hardly seen as positive, but we verify that they are positive by magnifying the figure. This positive slope at the origin is peculiar. It is caused by the asymmetry of the Lagrangian correlation function with respect to swapping the labelling and measuring times, t_ℓ and t_m, as discussed in Kraichnan (1966) and Gotoh *et al.* (1993) for the physical space. It can be shown that the slope at the origin, $\partial_{t_\ell} C_{jj}^{(L)}(\mathbf{k}, -\mathbf{k}, t_\ell \mid t_\ell, t_m)$ as $t_\ell \to t_m$ (from above), is equal to $\partial_{t_\ell} \langle |\hat{\mathbf{v}}(\mathbf{k}, t_\ell \mid t_m)|^2 \rangle / 2$ in the same limit. In order to observe how the Lagrangian modes change in time, we show the labelling-time evolution of the energy spectrum of the Lagrangian velocity in figure 10,
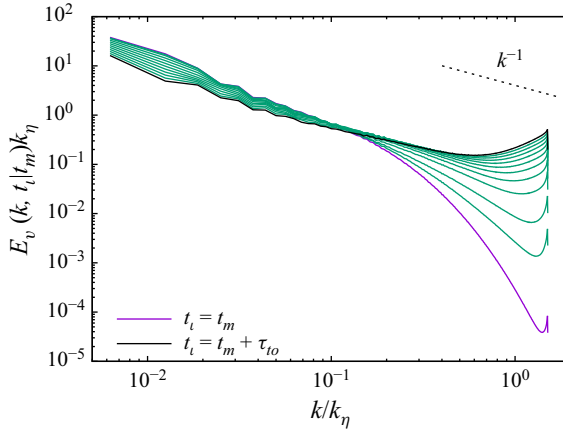
Figure 10. Labelling-time evolution of the energy spectrum of the Lagrangian velocity with $R_\lambda = 210$. The plotted curves' labelling times correspond to $t_\ell = t_m, t_m + 0.05\tau_{to}, t_m + 0.1\tau_{to}, t_m + 0.2\tau_{to}, \ldots, t_m + 1.0\tau_{to}$. We take neither temporal nor ensemble averages for each curve.

which is defined as

$$E_v(k, t_\ell \mid t_m) = \sum_{\substack{\boldsymbol{k} \\ k \leq |\boldsymbol{k}| < k + \Delta k}} \tfrac{1}{2} |\hat{\boldsymbol{v}}(\boldsymbol{k}, t_\ell \mid t_m)|^2, \tag{3.9}$$

where $\Delta k = 1$. As shown in figure 10, the Lagrangian spectrum $E_v(k, t_\ell \mid t_m)$ for large $k \, (\sim k_\eta)$ becomes much larger than the initial spectrum that is identical to the Eulerian energy spectrum. As explained in Kraichnan (1966) and Gotoh *et al.* (1993), the spectrum $E_v(k, t_\ell \mid t_m)$ for $k \geq k_\eta$, if it is fully numerically resolved, grows toward the k^{-1} spectrum by the same mechanism as the viscous–convective-range spectrum for the passive scalar. This growth corresponds to $\partial_{t_\ell}\langle|\hat{\boldsymbol{v}}(\boldsymbol{k}, t_\ell \mid t_m)|^2\rangle > 0$ at short times for large k and this implies $\partial_{t_\ell} C_{jj}^{(L)}(\boldsymbol{k}, -\boldsymbol{k}, t_\ell \mid t_\ell, t_m) > 0$ for large k. Therefore, the Lagrangian velocity correlation of large k grows at short times, as seen in figures 7(*a*) and 8. At the same time, the total kinetic energy of the Lagrangian velocity is conserved. To respect this conservation, the spectrum $E_v(k, t_\ell \mid t_m)$ for small k decreases, as seen in figure 10. This implies that $\partial_{t_\ell} C_{jj}^{(L)}(\boldsymbol{k}, -\boldsymbol{k}, t_\ell \mid t_\ell, t_m) < 0$ for small k at short times. Indeed, in our simulation, for the two smallest wavenumbers, $k = 1$ and 2, the slopes of the Lagrangian velocity correlation at the origin are negative (figure not shown).

Lastly, we observe that the FDT, $C^{(L)} \propto G^{(L)}$, is violated also in Lagrangian coordinates for all the wavenumbers shown in figure 7. In the Lagrangian coordinates, the response functions are larger than the correlation functions for small wavenumbers. In the Eulerian coordinates, the opposite is true, as shown in figure 1. The same tendency as in the Lagrangian coordinates, namely $G > C$, was observed in the shell model (Matsumoto *et al.* 2014). We do not have an explanation for this tendency in Lagrangian coordinates. Comparing the present result to that of the ALHDIA, we note that the difference between the Lagrangian correlation function and the response function obtained here is much larger than that of the ALHDIA for the inertial range, which was shown in figure 2 of Kraichnan (1966). The ALHDIA's two functions are nearly identical in the range of the vertical axis, $0.6 \leq G^{(L)} \leq 1.0$ and then they deviate from each other in $G^{(L)} \leq 0.6$. A possible explanation for this discrepancy between ours and the ALHDIA's is a finite Reynolds number effect since the ALHDIA treated the inertial-range quantities by setting $\nu = 0$.

Let us here comment on the FRR in Lagrangian coordinates. An FRR expression of the Lagrangian response function (3.3) analogous to the Eulerian FRRs cannot be obtained by adding the Gaussian random forcing to the right-hand side of the passive vector equation (3.1) in Fourier space. This is because the Lagrangian velocity measured at t_ℓ, which is in the numerator of (3.3), is not a solution to the passive vector equation. Instead, to obtain an FRR, we should add the Gaussian noise to the equation of the Lagrangian velocity $\boldsymbol{v}(\boldsymbol{a}, t_\ell \mid s_m)$, which describes the evolution in the measuring time s_m ranging from t_m to t_ℓ (see (B4) in Appendix B). Notice that this equation is different from the passive vector equation (3.1) describing the evolution in the labelling time. Under this setting, the Novikov–Carini–Quadrio FRR and the Harada–Sasa FRR for the Lagrangian response function are obtained on a formal level, as we describe in Appendix B. Contrary to the Eulerian case, numerical computation of these Lagrangian FRRs as they are is nearly impossible since it requires evaluation of the position function (Kaneda 1981). This is beyond the scope of our present study. Therefore we do not pursue numerical study of the Lagrangian FRRs here.

We end this section by describing the number of samples used in the calculation of the Lagrangian correlation functions and the response functions. The correlation functions shown in figure 7 are averaged in the following way. The length of the temporal window for calculating the correlation function is $1.67\tau_{to}$ and we take five consecutive windows from two simulations. Thus the total number of samples is 10. The response functions shown in figure 7 are averaged as follows. For the large wavenumbers, $k = k_\eta, k_\eta/2$ and $k_\eta/4$, the total number of samples is 20. Here, the length of the time windows are $0.333\tau_{to}$, $0.333\tau_{to}$ and $0.444\tau_{to}$, respectively. We take the 20 windows consecutively in one simulation. For the small wavenumbers, $k = k_\eta/8, k_\eta/16$ and $k_\eta/32$, the total number of samples are 20, 32 and 32, respectively. The window lengths are $0.556\tau_{to}$, $0.667\tau_{to}$ and $0.667\tau_{to}$, respectively. We place the windows consecutively in one simulation. As in the Eulerian case, we check the convergence of the correlation function and the response function by comparing the average over the full samples and some smaller samples. Here, we decrease the number of samples by $1/2$. The difference between the averages for the two sample data sets is within a few per cent for both the correlation function and the response function. In this sense, we regard that the correlation function and the response function have reached convergence.

In the resolution study, the correlation functions shown in figure 8 are averaged as follows. For the $k_{max}\eta = 1.5$ case with 256^3 grid points, we take 29 consecutive windows with the length $1.69\tau_{to}$ from one simulation. Hence, the total number of samples is 29. For the $k_{max}\eta = 3.0$ case with 512^3 grid points, we take 5 consecutive windows with the length 3.0 from one simulation. Hence, the total number of samples is 5. Although the sample sizes differ by approximately a factor 6, good agreement is observed. In the resolution study of the response function shown in figure 9, we use 128^3 and 256^3 grid points. We take the windows of the following sizes, $0.430\tau_{to}$, $0.538\tau_{to}$, $1.08\tau_{to}$ and $1.08\tau_{to}$, for $k = k_\eta, k_\eta/2, k_\eta/4$ and $k_\eta/8$, respectively. The number of the windows are 30 for $k = k_\eta, k_\eta/2$ and 60 for $k_\eta/4, k_\eta/8$. The windows are placed consecutively in one simulation. This setting is the same for the two resolutions.

4. Scaling of characteristic times associated with the correlation and response functions in the Eulerian and Lagrangian coordinates

Having measured the correlation functions and the linear response functions in both Eulerian and Lagrangian coordinates, we evaluate the characteristic times associated with them. The purpose is to identify how they vary as a function of wavenumber.
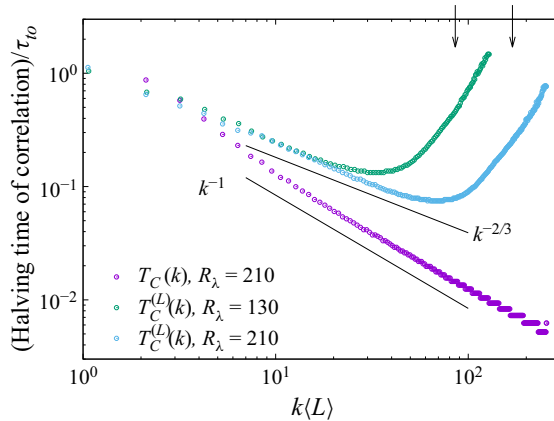
Figure 11. Halving time of the correlation function as a function of wavenumber k. The halving time of the Eulerian correlation function, $C_{\varphi\varphi}(k, t-s)$, and that of Lagrangian one, $C^{(L)}(k, t_\ell - t_m)$ are denoted by $T_C(k)$ and $T_C^{(L)}(k)$, respectively. For the Lagrangian halving time, we plot also the small Reynolds number case calculated with $k_{max}\eta = 1.5$, whose correlation functions were shown in figure 8. The wavenumber is normalised with the integral scale, $\langle L \rangle \simeq 1.05$, for both Reynolds number cases. The arrows in the top right corner indicate the Kolmogorov dissipation wavenumbers, k_η, of both cases. The halving time is normalised with the large-scale eddy turnover time, τ_{to}. The staircase-like behaviour of the Eulerian halving time, $T_C(k)$, for large k values is caused by the fact that the sampling of the correlation function becomes too coarse to resolve the halving time accurately. The Eulerian halving time at the smallest wavenumber, $T_C(k=1)$, is not measurable within the size of the temporal window used here since the Eulerian correlation at the smallest wavenumber, $k = 1$, does not decrease by one half.

Here, as a characteristic time, we consider the halving time, at which the function becomes one half of the value at the time origin. There are two reasons for this choice. One is that the halving time of the linear response function of the shell model was found to be statistically stable in quantifying its decrease by Biferale *et al.* (2001). The other reason concerns the similarity assumption made in solving the integro-differential equations obtained in the DIA-type closures as we briefly discussed in the Introduction. For this, we intend to focus on characteristic times representing the inertial range. They are intermediate in the sense that they are smaller than the large-scale turnover time and larger than the Kolmogorov dissipation time. Notice that obtaining the two functions up to the large-scale turnover time accurately is quite demanding since it requires a huge number of samples. The halving time is a good numerical compromise.

We calculate the halving time of the Eulerian correlation function $C_{\varphi\varphi}(k, t-s)$, which was already shown in figure 1, and of the Lagrangian correlation function $C^{(L)}(k, t_\ell - t_m)$, which was shown in figures 7 and 8. We denote the Eulerian and Lagrangian halving times of the correlations by $T_C(k)$ and $T_C^{(L)}(k)$, respectively. The results are plotted in figure 11. Some caution is needed to interpret the Lagrangian characteristic time, $T_C^{(L)}(k)$. We show two data sets with different Reynolds numbers for the Lagrangian halving time. Both exhibit the decreasing part and the increasing part. As we raise the Reynolds number, the range of the decreasing part in figure 11, which behaves as $k^{-2/3}$, becomes larger. Hence, we conclude that the Lagrangian characteristic time follows the Kolmogorov scaling, $T_C^{(L)}(k) \propto k^{-2/3}$, in the inertial range.

In Kaneda *et al.* (1999), the characteristic time of the Lagrangian velocity correlation at short times was studied with the Taylor expansion of the correlation function. Although their Lagrangian velocity, which evolves in the measuring time, and their definition of

the characteristic time are different from ours, they observed $k^{-2/3}$ behaviour of their characteristic time at short times if k is in the inertial range.

We consider the increasing part of $T_C^{(L)}(k)$ (which is close to k^2) as follows. First, it is in the large-wavenumber region, $k\langle L\rangle > 0.47k_\eta$. Let us look back at the graphs of the Lagrangian correlation functions shown in figure 7(*a*). We observed that the correlation functions for the corresponding wavenumbers, $k = k_\eta$ and $k_\eta/2$, grow at short time $t_\ell - t_m$, as we discussed in § 3. As a result, we have a much larger $T_C^{(L)}(k)$ at large k values than those at small k values, as inferred from figure 7(*a*). Because of this steep growth of the correlations, the meaning of the halving times for large k values is likely to be different from that of the halving times for the smaller wavenumbers $k < k_\eta/2$. In Kaneda *et al.* (1999), they observed a similar rapid growth in the large k region of their short-time characteristic time of the Lagrangian measuring-time evolved velocity correlation. They showed that the high-k growth is due to the viscosity from the equations for the Taylor coefficients. In our case, the rapid growth of $T_C^{(L)}(k)$ is considered to occur in the large-wavenumber range $k \sim k_\eta$, where the Lagrangian correlation grows at short times. This wavenumber range corresponds to the 'viscous–convective' range for the Lagrangian-history velocity. Hence, we infer that the high-k growth of $T_C^{(L)}(k)$ is due to lack of dissipation in the passive vector equations (3.1).

In contrast to the behaviour of the Lagrangian halving time $T_C^{(L)}(k)$, we observe that the Eulerian halving time follows $T_C(k) \propto k^{-1}$. Moreover, this k^{-1} behaviour covers not only the inertial range, but also the dissipation range. These power laws for the correlation functions are as expected and already obtained numerically, see e.g. Kraichnan (1964*b*) and Gotoh *et al.* (1993). The Eulerian time scale $T_C(k) \propto k^{-1}$ is known as the sweeping-time scaling and the Lagrangian time scale $T_C^{(L)}(k) \propto k^{-2/3}$ is the time scale of the Kolmogorov dimensional analysis in the inertial range, namely $\epsilon^{-1/3}k^{-2/3}$. From figure 11, we cannot rule out deviations of $T_C(k)$ from k^{-1} and of $T_C^{(L)}(k)$ from $k^{-2/3}$ in the inertial range, which may be due to some subdominant effect or due to the intermittency effect. The latter effect can be weak, if it exists, since we are treating the second-order moments. The non-dimensional constants involved in the characteristic times are estimated in the scaling range with the naked eye as $T_C(k) = 1.3/(ku_{rms})$ and $T_C^{(L)}(k) = 0.90\epsilon^{-1/3}k^{-2/3}$. Here, u_{rms} is the root-mean square Eulerian velocity. A similar k^{-1} behaviour was obtained for the characteristic time of the Eulerian velocity correlation at short times in Kaneda *et al.* (1999).

In figure 12, we plot the halving time of the Eulerian response function $G_{\varphi\varphi}(k, t - s)$, which was already shown in figure 1, and of the Lagrangian response function $G^{(L)}(k, t_\ell - t_m)$, which was shown in figure 7. We denote their time scales as $T_G(k)$ and $T_G^{(L)}(k)$, respectively. The number of sampling wavenumbers is only six since the numerical calculation of the response functions are very costly. The variation of the halving time of the Eulerian response functions is $T_G(k) \propto k^{-1}$ up to the dissipation range. For the Lagrangian response functions, we observe that the variation is close to $T_G^{(L)}(k) \propto k^{-2/3}$ except for the rightmost data for each R_λ, which are probably affected by the viscous dissipation. We also notice for $T_G^{(L)}(k)$ that small deviations from $k^{-2/3}$ is present. The non-dimensional constants in the scaling range are estimated with the naked eye as $T_G(k) = 1.1/(ku_{rms})$ and $T_G^{(L)}(k) = 1.1\epsilon^{-1/3}k^{-2/3}$.

We conclude that the time scale of the response function obeys the same scaling laws as that of the correlation function of the corresponding coordinates. While we have seen
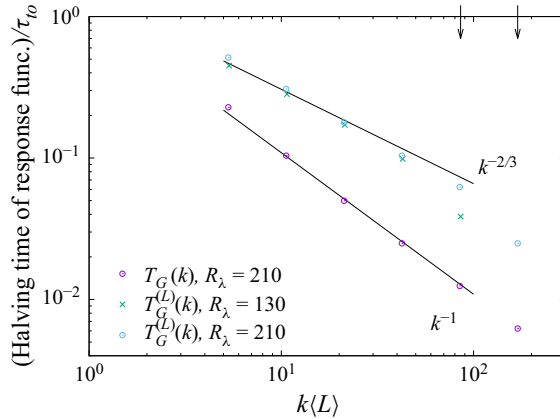
Figure 12. Halving time of the linear response function as a function of k. The halving time of the Eulerian response function, $G_{\varphi\varphi}(k, t - s)$, and that of the Lagrangian one, $G^{(L)}(k, t_\ell - t_m)$, are denoted by $T_G(k)$ and $T_G^{(L)}(k)$, respectively. As in figure 11, we plot the Lagrangian halving time of the small Reynolds number case calculated with $k_{max}\eta = 1.5$.

that the FDT, $C \propto G$, holds in neither coordinates, the characteristic times of the two functions follow the same scaling laws in k. This numerical result supports the self-similar assumptions made upon solving the integro-differential equations of the Eulerian DIA and the ALHDIA. To check the robustness of these scaling laws, instead of the halving time, we calculate the 3/4-time at which the correlation function and the response function decrease to 3/4 of the value at the time origin. Using the 3/4 time, we observe the same scaling laws as shown in figures 11 and 12.

In the numerical calculation of the Harada–Sasa FRR in Eulerian coordinates, we pointed out the twofold cancellation. In the description of the cancellation, we presented figure 4, where the triple correlation $L_\varphi(k, t, s)$ has a maximum and $L_\varphi(k, s, t)$ has a minimum for $t > s$. A characteristic time of $L_\varphi(k, t, s)$ can be obtained as the time at which $L_\varphi(k, t, s)$ becomes maximum or as the time at which $L_\varphi(k, s, t)$ becomes minimum. We plot these times as a function of k and find that they vary as k^{-1} (figure not shown). This indicates that this characteristic time of the energy transfer correlation $L_\varphi(k, t, s)$ has the sweeping scaling, as in the Eulerian correlation and response functions. We also plot the maximum values of $L_\varphi(k, t, s)$ and the absolute values of the minimum of $L_\varphi(k, s, t)$ as a function of k and find that they do not follow a power law of k.

5. Discussion

In Eulerian coordinates, we have calculated the linear response function in the deterministic case with the method used in Biferale *et al.* (2001). We have called it the direct method. In contrast, for the two FRRs, we have needed to add Gaussian random forcing. If the random forcing is sufficiently small, we have shown that the two FRRs agree with the response function in the deterministic setting calculated with the direct method, at least for large wavenumbers.

The following question then arises: Which way of calculating the response function in the deterministic setting is numerically the best for Navier–Stokes turbulence? In terms of yielding the least fluctuating results, the direct method is the best and the

Novikov–Carini–Quadrio FRR is the second best. Due to the twofold cancellations, the Harada–Sasa FRR is the worst. However, there is a price to pay for each approach. The FRRs allow one to compute the shell-averaged response function for all of the wavenumber shells at one time, in principle (apart from the statistical convergence). The drawback is that we need to identify how small the noise should be in order for the response function with the noise to agree with the response function without the noise. The direct method requires us to simultaneously follow two neighbouring solutions of the Navier–Stokes equations to compute one shell-averaged response function for a given wavenumber. To obtain the response function for a different wavenumber shell, we have to repeat this calculation by changing the shell to which we add the initial perturbation. This is more numerically expensive than following one solution of the randomly forced Navier–Stokes equations. However, our evaluation that the Harada–Sasa FRR underperforms in calculation of the linear response function of the Navier–Stokes turbulence ignores its physical significance in microscopic systems, which connects the hard-to-measure heat dissipation to other easy-to-measure statistical quantities and identifies the dissipation as the deviation from the FDT (for this, see, e.g. Puglisi *et al.* 2017).

Apart from the numerical convergence problem of the FRRs, the next question we address is the following: Can the FRRs yield a better understanding of turbulence than otherwise available? At present, we are not able to answer yes. Our numerical results suggested that the FRRs contain more information than the FDT does. In particular, the twofold cancellations of the Harada–Sasa FRR indicated that the deviation from the FDT is caused by both the nonlinearity and the dissipation. Whether or not the effect of the dissipation diminishes as we increase the Reynolds number, as suggested by the shell-model study (Matsumoto *et al.* 2014), remains to be seen. If the nonlinear part of the Harada–Sasa FRR, which corresponds to the energy transfer function at equal times, becomes dominant at high Reynolds numbers, it is tempting to connect the breakdown of the FDT with the energy cascade.

Granted that our current use of FRRs does not improve closure approximations, the FRRs' closed expressions of the response function, such as (2.13) and (2.15), in which no closure approximation is made, stimulate further analysis or comparison concerning assumption or consequence of a closure theory. As one example of such attempts, in Appendix D we study a short-time behaviour of the response function with the Novikov–Carini–Quadrio FRR by applying the field-theoretical method as used, for example, in Reichman & Charbonneau (2005). Such studies can be done not only in Eulerian coordinates but also in Lagrangian coordinates with both time orderings $t_\ell \geq t_m$ and $t_\ell \leq t_m$. As shown in Appendix D, we express the temporal Taylor expansion of the response functions, more precisely the Novikov–Carini–Quadrio FRRs, up to the second order in terms of the instantaneous two-point correlation functions. These expressions become independent of the temperature of the noise at short times, suggesting that such an analysis is meaningful also for studying the response function in a deterministic setting. Therefore, we consider that this line of research can yield an important insight only obtainable with the FRR. With the short-time expansion of the response function, we can study the dominant time scale of the response function in the inertial range. The results suggest that the sweeping scaling is dominant at short times for the Eulerian response function (Appendix C) and that the Kolmogorov scaling is dominant for Lagrangian response function in $t_m > t_\ell$ (Appendix D). However, for the Lagrangian-history response function $t_\ell > t_m$, the time scale at short times depends on the ultra-violet cutoff wavenumber (Appendix D). How the Kolmogorov scaling becomes

dominant in the half-life of the Lagrangian-history response function as observed in § 4, is an interesting theoretical problem.

Another way of going further with the FRRs can be to relax the constraint of sufficiently small noise. With a moderately large noise, the statistical quantities of the velocity field like the energy spectrum differ measurably from the deterministic case. If we tolerate this discrepancy, we can explore non-equilibrium characteristics using the FRRs (and recent fluctuation relations) numerically with various techniques of statistical mechanics. It should be noticed that, without the random forcing, obtaining a FRR-like exact expression of the linear response function in terms of the correlation functions is a challenge.

We have calculated the Lagrangian correlation function and the linear response function with the passive vector method. Despite the large truncation error of the Lagrangian velocity, we have obtained reliable numerical results from small to moderate wavenumbers. The characteristic times of the Lagrangian functions measured as the halving times obey the Kolmogorov scaling, $k^{-2/3}$, in the inertial range. This supports the assumption made in solving the integro-differential equations of the ALHDIA. In contrast, the characteristic times of the Eulerian correlation and response functions have the sweeping scaling k^{-1}. This Eulerian result is also consistent with the analysis made upon studying the failure of the Eulerian DIA, see, e.g. Kraichnan (1964*b*). There was an attempt to circumvent the failure within the Eulerian framework by assuming that the Eulerian response function has the Kolmogorov scaling $k^{-2/3}$ as the characteristic time, see § 6.4 of Leslie (1973). This assumption is not valid according to the numerical result obtained here.

We have observed that, for the FDT, the proportionality between the correlation function and the linear response function, does not hold in Eulerian coordinates and the 'abridged Lagrangian-history coordinates' where the labelling time is the present and the measuring time is the past, $t_\ell \geq t_m$. This is a manifestation of the non-Gaussian, non-equilibrium statistical mechanical character of turbulence (Marconi *et al.* 2008). These breakdowns of the FDT are consistent with the original Eulerian DIA and the ALHDIA, although the two DIAs lead to the FDT in the absolute equilibrium case or the fully thermalised Galerkin-truncated Euler case. On the other hand, the characteristic times of the correlation and linear response functions obey the same power-law scaling. In this sense, the discrepancy may not be taken so seriously.

In fact, our original motivation of this study was to numerically examine the FDT that holds as a consequence of the LRA and the LDIA. However, the Lagrangian quantities used in the LRA and the LDIA are hard to calculate with spectral accuracy. To aim at this accuracy we hence employ the passive vector method. Then, the price to pay for accuracy is the time ordering, $t_\ell \geq t_m$. In the LRA and the LDIA, the ordering is the opposite, i.e. $t_m \geq t_\ell$. Numerical study of the same ordering of the LRA and the LDIA can be done by adopting the Lagrangian particle tracking method as pioneered by Yeung & Pope (1989). We speculate that a similar breakdown of the FDT occurs in $t_m \geq t_\ell$ and that the characteristic times of the two functions follow the same scaling $k^{-2/3}$. As a further remark on the FDT in the LRA and the LDIA, the solenoidal projection of the measuring-time evolving Lagrangian velocity and the linear response function lead to the simplified closure equations as described in, e.g. Kaneda (2007). For the compressible components, the FDT may be broken even within the LRA and the LDIA.

For the Eulerian correlation function and the linear response function, we have estimated their characteristic times as $T_C(k) = 1.3/(ku_{rms})$ and $T_G(k) = 1.1/(ku_{rms})$, which are defined as the halving time. Here, one of the referees pointed out that the Gaussian function $\exp[-k^2 u_{rms}^2 (t-s)^2/2]$ has the halving time $\sqrt{2\log 2}/(ku_{rms}) \simeq 1.18/(ku_{rms})$,

which is close to the estimated characteristic times. Certainly, this Gaussian function with the sweeping scaling yields a fair approximation both to the Eulerian correlation functions and the linear response functions shown in figure 1, provided that we ignore the breakdown of the FDT.

6. Concluding remarks

We have numerically studied the correlation function and the linear response function both in Eulerian and Lagrangian coordinates in homogeneous isotropic turbulence with moderate Reynolds numbers.

In Eulerian coordinates, the directly measured response function was compared numerically to the two FRRs. With the sufficiently small amplitude of the Gaussian random forcing, the two FRRs agreed with the directly measured response function in the deterministic setting for the large and moderate wavenumbers. For the small wavenumbers we expect that they will agree better by increasing the number of statistical samples. In the Lagrangian coordinates, the correlation function and the linear response function were numerically obtained with the passive vector method for the time ordering $t_\ell \geq t_m$. In particular, the Lagrangian response function was calculated with DNS for the first time. The Lagrangian FRRs were considered only theoretically in the appendices since they involve the position function that is beyond the scope of the present DNS study.

Having calculated the two functions in both coordinates, we studied their characteristic times as a function of the wavenumber. The Eulerian times obey the sweeping scaling, k^{-1}. The Lagrangian times follow the Kolmogorov scaling, $k^{-2/3}$, in the inertial range, which is consistent with the assumption of the ALHDIA. All these results in both coordinates are as expected. However, these scaling laws of the characteristic times in the Lagrangian coordinates were verified numerically for the first time. To illustrate a possible use of the FRRs, in the appendices we calculate theoretically the time scales of the FRR expression of the response function at short times and discuss their dominant scaling in the inertial range.

We have considered the Eulerian and Lagrangian velocity statistics separately and have not addressed how they are related each other. The problem is a substantial challenge, as pointed out by He, Jin & Yang (2017) among many issues reviewed therein concerning two-point and two-time velocity correlations. An exact relation between the Eulerian and Lagrangian correlation functions of the velocity Fourier modes can be obtained by using the passive vector equation or the position function. The exact one can then be reduced to a closed relation between, for example, the Eulerian and Lagrangian characteristic times. To do this, we need to apply a closure approximation to the exact relation which involves third-order correlations, which is beyond the scope of this paper.

The linear response function has been employed mostly in DIA-type closure approximations. Our present study here is not directly relevant to developing a new closure approximation that is manageable for inhomogeneous and anisotropic turbulence. We recall that the classical role of the linear response function with the FDT is to describe how a system in the thermal equilibrium state responds to a small perturbation and how it comes back to the equilibrium state. Much beyond the classical role, the FRRs have been developed to describe non-equilibrium systems which include Navier–Stokes turbulence, as we studied. We hope that these non-equilibrium FRRs will reveal the unknown non-equilibrium character of turbulent flow and lead to its better understanding.

Author ORCIDs.
- Takeshi Matsumoto https://orcid.org/0000-0002-4529-145X;
- Michio Otsuki https://orcid.org/0000-0001-5947-8621;
- Takeshi Ooshida https://orcid.org/0000-0002-3276-0122;
- Susumu Goto https://orcid.org/0000-0001-7013-7967.

Appendix A. Derivation of the Harada–Sasa FRR in Eulerian coordinates

We derive the FRR (2.15) by applying the formalism proposed by Harada & Sasa (2005, 2006) to the Navier–Stokes equations (2.10). The starting point of this formalism is the transition probability of the Gaussian random forcing, $(\hat{\xi}_\varphi(\boldsymbol{k}, t), \hat{\xi}_\theta(\boldsymbol{k}, t))$, from one state at time t_0 to another at time t. It can be written as a path-integral form of the corresponding Brownian paths,

$$P(\boldsymbol{\Xi}_0, t_0 \mid \boldsymbol{\Xi}, t) = \int_{(\boldsymbol{\Xi}_0, t_0)}^{(\boldsymbol{\Xi}, t)} D[\boldsymbol{\Xi}] \exp\left(-\frac{1}{2} \sum_{\boldsymbol{k}} \int_{t_0}^{t} \mathrm{d}s \frac{|\hat{\xi}_\varphi(\boldsymbol{k}, s)|^2 + |\hat{\xi}_\theta(\boldsymbol{k}, s)|^2}{\sigma^2(k)T} \right). \quad \text{(A1)}$$

Here, $\boldsymbol{\Xi}$ denotes one instantaneous realisation of the random forcing for all $\boldsymbol{k}$ values and $D[\boldsymbol{\Xi}]$ represents a measure associated with a Brownian path. To consider the linear response, we next add a probe force $(f_\varphi^{(p)}(\boldsymbol{k}, t), f_\theta^{(p)}(\boldsymbol{k}, t))$ to the right-hand side of the Navier–Stokes equations (2.10). This probe force is infinitesimally small. Now we change variables from the random forcing $\boldsymbol{\Xi}$ to the velocity $\boldsymbol{U}$, which denotes all the velocity Fourier modes. This results in

$$P(\boldsymbol{U}_0, t_0 \mid \boldsymbol{U}, t) = \int_{(\boldsymbol{U}_0, t_0)}^{(\boldsymbol{U}, t)} D[\boldsymbol{U}] \exp\Bigg[-\sum_{\boldsymbol{k}} \frac{1}{2\sigma^2(k)T} \int_{t_0}^{t} \mathrm{d}s \left(|\dot{\hat{u}}_\varphi(\boldsymbol{k}, s) - \Lambda_\varphi(\boldsymbol{k}, s) \right.$$

$$+ \nu k^2 \hat{u}_\varphi(\boldsymbol{k}, s) - f_\varphi^{(p)}(\boldsymbol{k}, s)|^2 + |\dot{\hat{u}}_\theta(\boldsymbol{k}, s)$$

$$\left. - \Lambda_\theta(\boldsymbol{k}, s) + \nu k^2 \hat{u}_\theta(\boldsymbol{k}, s) - f_\theta^{(p)}(\boldsymbol{k}, s)|^2 \right) \Bigg] \mathcal{J}, \quad \text{(A2)}$$

where $\dot{\hat{u}}$ denotes the time derivative of $\hat{u}$ and $\mathcal{J}$ is the Jacobian due to the change of variables. With this probability, we formally write the mean of $\hat{u}_\varphi(\boldsymbol{k}, t)$ in the presence of

the probe force, which is denoted by $\langle \hat{u}_\varphi(\boldsymbol{k}, t) \rangle_p$, as

$$
\langle \hat{u}_\varphi(\boldsymbol{k}, t) \rangle_p = \int_{(U_0, t_0)}^{(U,t)} D[U] \hat{u}_\varphi(\boldsymbol{k}, t) \exp \Bigg[- \sum_{\boldsymbol{k}} \frac{1}{2\sigma^2(k)T} \int_{t_0}^{t} \mathrm{d}s \left(|\dot{\hat{u}}_\varphi(\boldsymbol{k}, s) - \Lambda_\varphi(\boldsymbol{k}, s) \right.
$$

$$
+ \nu k^2 \hat{u}_\varphi(\boldsymbol{k}, s) - f_\varphi^{(p)}(\boldsymbol{k}, s)|^2 + |\dot{\hat{u}}_\theta(\boldsymbol{k}, s)
$$

$$
\left. - \Lambda_\theta(\boldsymbol{k}, s) + \nu k^2 \hat{u}_\theta(\boldsymbol{k}, s) - f_\theta^{(p)}(\boldsymbol{k}, s)|^2 \right) \Bigg] \mathcal{J} \tag{A3}
$$

(if needed, one can further take the average over the initial velocity U_0 at time t_0 by specifying the probability distribution of U_0). We then expand this mean velocity up to the first order of the probe force as

$$
\langle \hat{u}_\varphi(\boldsymbol{k}, t) \rangle_p \simeq \int_{(U_0, t_0)}^{(U,t)} D[U] \exp \Bigg[- \sum_{\boldsymbol{q}} \frac{1}{2\sigma^2(q)T} \int_{t_0}^{t} \mathrm{d}s \left(|\dot{\hat{u}}_\varphi(\boldsymbol{q}, s) - \Lambda_\varphi(\boldsymbol{q}, s) \right.
$$

$$
\left. + \nu q^2 \hat{u}_\varphi(\boldsymbol{q}, s)|^2 + |\dot{\hat{u}}_\theta(\boldsymbol{q}, s) - \Lambda_\theta(\boldsymbol{q}, s) + \nu q^2 \hat{u}_\theta(\boldsymbol{q}, s)|^2 \right) \Bigg] \mathcal{J} \times \hat{u}_\varphi(\boldsymbol{k}, t)
$$

$$
\times \Bigg\{ 1 + \sum_{\boldsymbol{q}} \frac{1}{\sigma^2(q)T} \int_{t_0}^{t} \mathrm{d}s \left[\dot{\hat{u}}_\varphi(\boldsymbol{q}, s) - \Lambda_\varphi(\boldsymbol{q}, s) + \nu q^2 \hat{u}_\varphi(\boldsymbol{q}, s) \right]^* f_\varphi^{(p)}(\boldsymbol{q}, s)
$$

$$
+ \left[\dot{\hat{u}}_\theta(\boldsymbol{q}, s) - \Lambda_\theta(\boldsymbol{q}, s) + \nu q^2 \hat{u}_\theta(\boldsymbol{q}, s) \right]^* f_\theta^{(p)}(\boldsymbol{q}, s) \Bigg\}. \tag{A4}
$$

Here, we assume that $\mathcal{J}$ does not contribute to this form and ignore formally the first-order term of the complex conjugate of the probe force. Notice that the first term (i.e. the zeroth-order term) in the integrand of (A4) is

$$
\langle \hat{u}_\varphi(\boldsymbol{k}, t) \rangle = \int_{(U_0, t_0)}^{(U,t)} D[U] \exp \Bigg[- \frac{1}{2\sigma^2(k)T} \sum_{\boldsymbol{q}} \int_{t_0}^{t} \mathrm{d}s \left(|\dot{\hat{u}}_\varphi(\boldsymbol{q}, s) - \Lambda_\varphi(\boldsymbol{q}, s) + \nu q^2 \hat{u}_\varphi(\boldsymbol{q}, s)|^2 \right.
$$

$$
\left. + |\dot{\hat{u}}_\theta(\boldsymbol{q}, s) - \Lambda_\theta(\boldsymbol{q}, s) + \nu q^2 \hat{u}_\theta(\boldsymbol{q}, s)|^2 \right) \Bigg] \mathcal{J} \times \hat{u}_\varphi(\boldsymbol{k}, t), \tag{A5}
$$

where $\langle \cdot \rangle$ denotes the average under the setting without the probe force. Since $\delta \hat{u}_\varphi(\boldsymbol{k}, t) = \langle \hat{u}_\varphi(\boldsymbol{k}, t) \rangle_p - \langle \hat{u}_\varphi(\boldsymbol{k}, t) \rangle$, the expansion (A4) and (A5) yields the expression of the mean linear response function

$$
\frac{\delta \hat{u}_\varphi(\boldsymbol{k}, t)}{\delta f_\varphi^{(p)}(\boldsymbol{q}', s')} = \frac{1}{2\sigma^2(q)T} \langle \hat{u}_\varphi(\boldsymbol{k}, t) \left[\dot{\hat{u}}_\varphi(\boldsymbol{q}', s') - \Lambda_\varphi(\boldsymbol{q}', s') + \nu q^2 \hat{u}_\varphi(\boldsymbol{q}', s') \right]^* \rangle. \tag{A6}
$$

919 A9-31

We can eliminate the time-derivative term for the diagonal component, $q' = k$, in the following manner. For $t \geq s$, the diagonal component can be written as

$$\frac{\delta \hat{u}_\varphi(k, t)}{\delta f_\varphi^{(p)}(k, s)} = \frac{1}{2\sigma^2(k)T} \left[\partial_s \langle \hat{u}_\varphi(k, t) \hat{u}_\varphi^*(k, s) \rangle - \langle \Lambda_\varphi^*(k, s) \hat{u}_\varphi(k, t) \rangle \right.$$
$$\left. + \nu k^2 \langle \hat{u}_\varphi(k, t) \hat{u}_\varphi^*(k, s) \rangle \right]. \tag{A7}$$

Now we interchange t and s in (A7). Because of the causality, the left-hand side becomes zero

$$0 = \frac{1}{2\sigma^2(k)T} \left[\partial_t \langle \hat{u}_\varphi(k, s) \hat{u}_\varphi^*(k, t) \rangle - \langle \Lambda_\varphi^*(k, t) \hat{u}_\varphi(k, s) \rangle + \nu k^2 \langle \hat{u}_\varphi(k, s) \hat{u}_\varphi^*(k, t) \rangle \right]. \tag{A8}$$

Here, $\partial_t \langle \hat{u}_\varphi(k, s) \hat{u}_\varphi^*(k, t) \rangle = -\partial_s \langle \hat{u}_\varphi(k, t) \hat{u}_\varphi^*(k, s) \rangle$ since the autocorrelation function is a function of $t - s$ due to the statistical steadiness. Adding the two equations together, the diagonal component becomes

$$\frac{\delta \hat{u}_\varphi(k, t)}{\delta f_\varphi^{(p)}(k, s)} = \frac{1}{2\sigma^2(k)T} \left[2\nu k^2 \langle \hat{u}_\varphi(k, t) \hat{u}_\varphi^*(k, s) \rangle \right.$$
$$\left. - \langle \Lambda_\varphi^*(k, s) \hat{u}_\varphi(k, t) \rangle - \langle \Lambda_\varphi^*(k, t) \hat{u}_\varphi(k, s) \rangle \right], \tag{A9}$$

which is the Harada–Sasa FRR in Eulerian coordinates given in (2.15).

Appendix B. Derivation of the Novikov–Carini–Quadrio and Harada–Sasa FRRs in Lagrangian coordinates

We first recall the measuring-time evolution equations of the Lagrangian velocity, which involve the position function. The position function introduced by Kaneda (1981) is

$$\psi(x, t_m \mid a, t_\ell) = \delta(x - X(a, t_\ell \mid t_m)), \tag{B1}$$

with which the Lagrangian velocity is written through the Eulerian velocity as

$$v(a, t_\ell \mid t_m) = \int dx \, u(x, t_m) \psi(x, t_m \mid a, t_\ell). \tag{B2}$$

Let us write the Fourier series of the position function as

$$\psi(x, t_m \mid a, t_\ell) = \sum_{k,p} \hat{\psi}(k, t_m \mid p, t_\ell) \exp(i(k \cdot x + p \cdot a)). \tag{B3}$$

The measuring-time evolution equation of the Lagrangian velocity in Fourier space can be obtained from the Eulerian Navier–Stokes equations (2.1) as

$$\partial_{t_m} \hat{v}_j(k, t_\ell \mid t_m) = -(2\pi)^3 \nu \sum_p p^2 \hat{u}_j(p, t_m) \hat{\psi}(-p, t_m \mid k, t_\ell)$$
$$- i(2\pi)^3 \sum_p \sum_{\substack{q,r \\ q+r+p=0}} \frac{p_j p_a p_b}{p^2} \hat{u}_a(q, t_m) \hat{u}_b(r, t_m) \hat{\psi}(-p, t_m \mid k, t_\ell)$$
$$+ (2\pi)^3 \sum_p \hat{F}_j(p, t_m) \hat{\psi}(-p, t_m \mid k, t_\ell), \tag{B4}$$

where $p = |\boldsymbol{p}|$. The measuring-time evolution of the position function and the relation between the Eulerian and Lagrangian velocity modes are given by

$$\partial_{t_m}\hat{\psi}(\boldsymbol{k}, t_m \mid \boldsymbol{p}, t_\ell) = -\mathrm{i}k_j \sum_{\substack{\boldsymbol{p},\boldsymbol{q} \\ \boldsymbol{k}+\boldsymbol{p}+\boldsymbol{q}=0}} \hat{u}_j(-\boldsymbol{p}, t_m)\hat{\psi}(-\boldsymbol{q}, t_m \mid \boldsymbol{p}, t_\ell), \tag{B5}$$

$$\hat{u}_j(\boldsymbol{k}, t_m) = (2\pi)^3 \sum_{\boldsymbol{p}} \hat{v}_j(\boldsymbol{p}, t_\ell \mid t_m)\hat{\psi}(\boldsymbol{k}, t_m \mid -\boldsymbol{p}, t_\ell). \tag{B6}$$

This set of (B4)–(B6) is the same as derived by, for example, Kida & Goto (1997). Notice that DNS of these equations is nearly impossible because the degrees of freedom of the position function is prohibitively large. To obtain the FRRs, we consider the Lagrangian linear response function by adding the probe force $g_j^{(p)}(\boldsymbol{k}, t_\ell \mid t_m)$ and the Gaussian random force $\hat{\zeta}_j(\boldsymbol{k}, t_\ell \mid t_m)$ to the right-hand side of (B4). This addition of the random force is not the same as adding the Gaussian noise to the velocity of the Lagrangian particles.

As in the Eulerian case, let us set the mean and the covariance of the random forcing to

$$\langle \hat{\zeta}_j(\boldsymbol{k}, t_\ell \mid t_m) \rangle = 0, \tag{B7}$$

$$\langle \hat{\zeta}_j(\boldsymbol{k}, t_\ell \mid t_m)\hat{\zeta}_n(\boldsymbol{p}, t_\ell \mid t'_m) \rangle = 2\tilde{\sigma}^2(k)T\delta_{j,n}\delta_{\boldsymbol{k},-\boldsymbol{p}}\delta(t_m - t'_m), \tag{B8}$$

where $\tilde{\sigma}^2(k)$ is some function of k. The Novikov–Carini–Quadrio FRR in Lagrangian coordinates for $s \geq s'$ can be written as

$$\frac{\delta\hat{v}_j(\boldsymbol{k}, t_\ell \mid s)}{\delta\hat{g}_n^{(p)}(\boldsymbol{q}, t_\ell \mid s')} = \frac{1}{2\tilde{\sigma}^2(k)T}\langle \hat{v}_j(\boldsymbol{k}, t_\ell \mid s)\hat{\zeta}_n^*(\boldsymbol{q}, t_\ell \mid s') \rangle, \tag{B9}$$

by applying the method of Novikov (1965). The Harada–Sasa FRR in the Lagrangian coordinates can also be obtained in the same way as Appendix A, which reads

$$\frac{\delta\hat{v}_j(\boldsymbol{k}, t_\ell \mid s)}{\delta g_n^{(p)}(\boldsymbol{q}, t_\ell \mid s')} = \frac{1}{2\tilde{\sigma}^2(k)T}\left[\langle \hat{v}_j(\boldsymbol{k}, t_\ell \mid s)\{\partial_{s'}\hat{v}_n^*(\boldsymbol{p}, t_\ell \mid s')\}\rangle - \langle \tilde{\Lambda}_n^*(\boldsymbol{k}, t_\ell \mid s')\hat{v}_j(\boldsymbol{k}, t_\ell \mid s)\rangle\right]. \tag{B10}$$

Here, $\tilde{\Lambda}_j(\boldsymbol{k}, t_\ell \mid t_m)$ denotes the right-hand side of (B4).

Let us narrow down these expressions to those of the diagonal component ($j = n$ and $\boldsymbol{p} = \boldsymbol{k}$) with $s = t_\ell$ and $s' = t_m$ so that they become consistent with the response function (3.8). The Novikov–Carini–Quadrio FRR becomes

$$\frac{\delta\hat{v}_j(\boldsymbol{k}, t_\ell \mid t_\ell)}{\delta\hat{g}_j^{(p)}(\boldsymbol{k}, t_\ell \mid t_m)} = \frac{1}{2\tilde{\sigma}^2(k)T}\langle \hat{u}_j(\boldsymbol{k}, t_\ell)\hat{\zeta}_j^*(\boldsymbol{k}, t_\ell \mid t_m) \rangle. \tag{B11}$$

Here, we do not take summation over the index j. Although this looks simple, numerical calculation of the right-hand side of (B11) requires solving (B4) with the random forcing (more precisely, (D2) or (D5)). This is not an easy task. The Harada–Sasa FRR for the diagonal component becomes

$$\frac{\delta\hat{v}_j(\boldsymbol{k}, t_\ell \mid t_\ell)}{\delta\hat{g}_j^{(p)}(\boldsymbol{k}, t_\ell \mid t_m)} = \frac{1}{2\tilde{\sigma}^2(k)T}\left[\partial_{t_m}\langle \hat{u}_j(\boldsymbol{k}, t_\ell)\hat{v}_j^*(\boldsymbol{k}, t_\ell \mid t_m)\rangle - \langle \tilde{\Lambda}_j^*(\boldsymbol{k}, t_\ell \mid t_m)\hat{u}_j(\boldsymbol{k}, t_\ell)\rangle\right]. \tag{B12}$$

We cannot eliminate the time-derivative term in (B12) by using the same causality and symmetry argument made in the Eulerian case. Notice that the second term in (B12) involves correlations between the position function and the Eulerian velocity.

Appendix C. Short-time expansion of the Novikov–Carini–Quadrio FRR in Eulerian coordinates

We consider the Taylor expansion of the Novikov–Carini–Quadrio FRR in Eulerian coordinates at short time difference $\varepsilon \geq 0$,

$$G_{\alpha\alpha}^{(T)}(\boldsymbol{k}, t+\varepsilon \mid -\boldsymbol{k}, t) = \frac{1}{2\sigma^2(k)T}\langle \hat{u}_\alpha(\boldsymbol{k}, t+\varepsilon)\hat{\xi}_\alpha(-\boldsymbol{k}, t)\rangle = a_0 + a_1\varepsilon + a_2\varepsilon^2 + O(\varepsilon^3),$$
(C1)

where we do not take summation over the index α which is either φ or θ. We use the standard field-theoretical technique, although we do not employ a renormalisation procedure. In particular, we write the coefficients a_0, a_1 and a_2 in terms of the equal-time correlation functions of the Eulerian velocity Fourier modes. Then, we argue that the dominant scaling behaviour is $a_2 \propto k^2$ in the inertial range. This shows that the dominant time scale at short time is given by the sweeping scaling k^{-1}, as expected. In Kaneda (1993) and Kaneda *et al.* (1999), the Taylor expansion of the Eulerian and Lagrangian velocity correlations with the LRA and DNS data has been studied to identify the characteristic times from the second-order coefficients. In the current and next appendices, we consider the Taylor expansion of the Eulerian and Lagrangian linear response functions without using DNS data.

Now let us consider the Navier–Stokes equations in the following form:

$$\partial_t \hat{u}_\alpha(\boldsymbol{k}, t) = (e_\alpha(\boldsymbol{k}))_j \left(-\frac{\mathrm{i}}{2}\right) P_{jlm}(\boldsymbol{k}) \sum_{\substack{\boldsymbol{p}, \boldsymbol{q} \\ \boldsymbol{p}+\boldsymbol{q}+\boldsymbol{k}=\boldsymbol{0}}} \hat{u}_l(-\boldsymbol{p}, t)\hat{u}_m(-\boldsymbol{q}, t) - \nu k^2 \hat{u}_\alpha(\boldsymbol{k}, t)$$
$$+ \hat{F}_\alpha(\boldsymbol{k}, t) + \hat{\xi}_\alpha(\boldsymbol{k}, t),$$
(C2)

where $\hat{F}_\alpha(\boldsymbol{k}, t)$ is the large-scale forcing term. The Duhamel-type formal solution of (C2) is

$$\hat{u}_\alpha(\boldsymbol{k}, t+\varepsilon) = \mathrm{e}^{-\nu k^2 \varepsilon}\hat{u}_\alpha(\boldsymbol{k}, t) + \int_t^{t+\varepsilon} \exp(-\nu k^2(t+\varepsilon-s))\left[\Lambda_\alpha(\boldsymbol{k}, s) + \hat{\xi}_\alpha(\boldsymbol{k}, s)\right]\mathrm{d}s,$$
(C3)

where $\Lambda_\alpha(\boldsymbol{k}, s)$ denotes the nonlinear and the large-scale forcing terms in (C2). Using this form, the correlation between the velocity Fourier mode and the random forcing in the Novikov–Carini–Quadrio FRR can be written as

$$\langle \hat{u}_\alpha(\boldsymbol{k}, t+\varepsilon)\hat{\xi}_\alpha(-\boldsymbol{k}, t)\rangle = \mathrm{e}^{-\nu k^2 \varepsilon}\langle \hat{u}_\alpha(\boldsymbol{k}, t)\hat{\xi}_\alpha(-\boldsymbol{k}, t)\rangle$$
$$+ \int_t^{t+\varepsilon} \mathrm{d}s \, \exp(-\nu k^2(t+\varepsilon-s))\left[\langle \Lambda_\alpha(\boldsymbol{k}, s)\hat{\xi}_\alpha(-\boldsymbol{k}, t)\rangle + \langle \hat{\xi}_\alpha(\boldsymbol{k}, s)\hat{\xi}_\alpha(-\boldsymbol{k}, t)\rangle\right].$$
(C4)

In this calculation, we interpret the stochastic differential equation (C2) in the sense of Itô. So that we have

$$\langle \hat{u}_\alpha(\boldsymbol{p}, t)\hat{\xi}_\alpha(-\boldsymbol{k}, t)\rangle = 0,$$
(C5)

(which means that the noise generated at time t is independent of the velocity at the same time) and

$$\int_t^{t+\varepsilon} \exp(-\nu k^2(t+\varepsilon-s))\langle \hat{\xi}_\alpha(\boldsymbol{k}, s)\hat{\xi}_\alpha(-\boldsymbol{k}, t)\rangle \, \mathrm{d}s = \mathrm{e}^{-\nu k^2 \varepsilon}2\sigma^2(k)T,$$
(C6)

from the covariance (2.12). Therefore the velocity–noise correlation (C4) can be calculated as

$$
\langle \hat{u}_\alpha(\mathbf{k}, t+\varepsilon)\hat{\xi}_\alpha(-\mathbf{k}, t)\rangle = \mathrm{e}^{-\nu k^2 \varepsilon}\left[2\sigma^2(k)T + \int_t^{t+\varepsilon} \mathrm{e}^{-\nu k^2(t-s)}\langle \Lambda_\alpha(\mathbf{k}, s)\hat{\xi}_\alpha(-\mathbf{k}, t)\rangle\,\mathrm{d}s\right].
$$
(C7)

In what follows, we ignore the viscous term and the large-scale forcing term in order to discuss the inertial-range behaviour. The correlation in the integrand of (C7) is then

$$
\langle \Lambda_\alpha(\mathbf{k}, s)\hat{\xi}_\alpha(-\mathbf{k}, t)\rangle = (e_\alpha(\mathbf{k}))_j \tilde{P}_{jlm}(\mathbf{k}) \sum_{\substack{\mathbf{p},\mathbf{q} \\ \mathbf{p}+\mathbf{q}+\mathbf{k}=\mathbf{0}}} \langle \hat{u}_l(-\mathbf{p}, s)\hat{u}_m(-\mathbf{q}, s)\hat{\xi}_\alpha^*(\mathbf{k}, t)\rangle, \quad \text{(C8)}
$$

where we substitute the corresponding Duhamel solution for $\hat{u}_l(-\mathbf{p}, s)$ and $\hat{u}_m(-\mathbf{q}, s)$. Here, $\tilde{P}_{jlm}(\mathbf{k}) = (-\mathrm{i}/2)P_{jlm}(\mathbf{k})$. By repeating this procedure, we arrive at the expansion of the correlation (C4),

$$
\langle \hat{u}_\alpha(\mathbf{k}, t+\varepsilon)\hat{\xi}_\alpha(-\mathbf{k}, t)\rangle = 2\sigma^2 T
$$
$$
+ 4\varepsilon^2\sigma^2 T(e_\alpha(\mathbf{k}))_j(e_\alpha(\mathbf{k}))_c\tilde{P}_{jlm}(\mathbf{k})\sum_{\mathbf{p}}\tilde{P}_{mcd}(\mathbf{p}+\mathbf{k})\langle \hat{u}_l^*(\mathbf{p}, t)\hat{u}_d(\mathbf{p}, t)\rangle
$$

$$
+ O(\varepsilon^3) = 2\sigma^2 T - \varepsilon^2\left[2k_l(e_\alpha(\mathbf{k}))_d\sum_{\mathbf{p}}(\mathbf{p}\cdot e_\alpha(\mathbf{k}))\langle \hat{u}_l^*(\mathbf{p}, t)\hat{u}_d(\mathbf{p}, t)\rangle\right.
$$

$$
+ k_l k_d\sum_{\mathbf{p}}\left(1 - \frac{2(\mathbf{p}\cdot e_\alpha(\mathbf{k}))^2}{|\mathbf{p}+\mathbf{k}|^2}\right)\langle \hat{u}_l^*(\mathbf{p}, t)\hat{u}_d(\mathbf{p}, t)\rangle
$$

$$
\left. - 2k_d(e_\alpha(\mathbf{k}))_l\sum_{\mathbf{p}}(\mathbf{p}\cdot e_\alpha(\mathbf{k}))\frac{\mathbf{k}(\mathbf{k}+\mathbf{p})}{|\mathbf{k}+\mathbf{p}|^2}\langle \hat{u}_l^*(\mathbf{p}, t)\hat{u}_d(\mathbf{p}, t)\rangle\right] + O(\varepsilon^3). \quad \text{(C9)}
$$

To make it simpler, we further assume that the diagonal parts ($l = d$) are dominant. This leads to an expression of the Eulerian response function as

$$
G_{\alpha\alpha}^{(T)}(\mathbf{k}, t+\varepsilon \mid -\mathbf{k}, t) \simeq 1 - \frac{1}{2}\varepsilon^2 k^2\sum_{\mathbf{p}}\left(1 - \frac{2(\mathbf{p}\cdot e_\alpha(\mathbf{k}))^2}{|\mathbf{p}+\mathbf{k}|^2}\right)\langle|\hat{u}(\mathbf{p}, t)|^2\rangle + O(\varepsilon^3).
$$
(C10)

Clearly, the first term of the summand in (C10) represents the sweeping scaling. The scaling behaviour of the second term in the summand can be estimated in the inertial range by changing the summation to an integral and assuming the Kolmogorov scaling law, $\langle|\hat{u}(\mathbf{p}, t)|^2\rangle = C_K/(2\pi)\epsilon^{2/3}p^{-11/3}$ in the wavenumber range ($0 <)k_0 \leq p \leq k_1$. Here, C_K is the Kolmogorov universal constant and ϵ is the energy dissipation rate; k_0 and k_1 are

the wavenumber cutoffs. The second term in the summation can be estimated as follows

$$
k^2 \sum_{\boldsymbol{p}} \frac{(\boldsymbol{p} \cdot \boldsymbol{e}_\alpha(\boldsymbol{k}))^2}{|\boldsymbol{k}+\boldsymbol{p}|^2} \langle |\hat{\boldsymbol{u}}(\boldsymbol{p}, t)|^2 \rangle \simeq k^2 \left(\frac{L}{2\pi} \right)^3 \frac{C_K}{2\pi} \int_{k_0}^{k_1} \mathrm{d}p \int_0^\pi \mathrm{d}\theta
$$

$$
\times \int_0^{2\pi} \mathrm{d}\varphi \frac{p^4 \sin^3 \theta \cos^2 \varphi}{k^2 + p^2 + 2kp \cos \theta} \epsilon^{2/3} p^{-11/3}
$$

$$
= \frac{1}{2} C_K \epsilon^{2/3} \int_{k_0}^{k_1} \mathrm{d}p \, p^{1/3} \left[\frac{k^2 + p^2}{2p^2} - \frac{(p^2 - k^2)^2}{4kp^3} \log \frac{p+k}{|p-k|} \right]
$$

$$
= -\frac{9\sqrt{3}}{35} \pi C_K \epsilon^{2/3} k^{4/3} + \text{(subleading terms).} \tag{C11}
$$

Here, we set $\boldsymbol{p} \cdot \boldsymbol{e}_\alpha(\boldsymbol{k}) = p \sin \theta \cos \varphi$, where we regard $\boldsymbol{k} = (0, 0, 1)$ and $\boldsymbol{e}_\alpha = (1, 0, 0)$ and the box size is $L = 2\pi$. The integral in the second line of (C11) can be calculated analytically. From that result, we calculate the leading behaviour of (C11) by assuming $k_0 \ll k \ll k_1$.

Therefore, the Novikov–Carini–Quadrio FRR leads to the following expansion of the Eulerian response function in the inertial range:

$$
G_{\alpha\alpha}^{(T)}(\boldsymbol{k}, t + \varepsilon \mid -\boldsymbol{k}, t) \simeq 1 - \varepsilon^2 \left[\langle E \rangle k^2 - \frac{9\sqrt{3}}{35} \pi C_K \epsilon^{2/3} k^{4/3} \right] + O(\varepsilon^3)
$$

$$
\simeq 1 - \frac{\varepsilon^2}{2} \left[3u_{rms}^2 k^2 - \frac{18\sqrt{3}}{35} \pi C_K \epsilon^{2/3} k^{4/3} \right] + O(\varepsilon^3), \tag{C12}
$$

where the energy is $\langle E \rangle = \sum_{\boldsymbol{p}} \langle |\hat{\boldsymbol{u}}(\boldsymbol{p}, t)|^2 \rangle / 2$ and u_{rms} is the root-mean-square of the velocity defined as $u_{rms} = (2\langle E \rangle / 3)^{1/2}$. Hence, the short-time characteristic time of the Eulerian response function is indeed the sweeping-time scaling, $(ku_{rms})^{-1}$. Here the Kolmogorov-time scaling $\epsilon^{-1/3} k^{-2/3}$ is present but subdominant. The result (C12) can be compared to a theoretical result in Kaneda (1993), $G^{(T=0)} = 1 - (\varepsilon^2/2)[k^2 u_{rms}^2 - 1.66\epsilon^{2/3} k^{4/3}] + O(\varepsilon^3)$, obtained as the time expansion for the Eulerian velocity correlation function. For comparison, we need to assume the FDT, contrary to what we find in § 2. The numerical constants in (C12) are larger than those of Kaneda's result. The prefactor in (C12) of the Kolmogorov-time scaling can be estimated as $(18\sqrt{3}/35)\pi C_K \simeq 2.80 C_K = 4.76$ using an estimate of the Kolmogorov constant $C_K = 1.70$.

The viscous term brings a linear term of ε in the short time expansion of the response function, as seen in (C7). There is also a viscous correction in the second-order term of ε, which is ignored here.

As we have seen, up to the second order, the coefficients of the expansion do not depend on the noise covariance. If the expansion (C1) is continued to higher orders of ε, it is expected that the coefficients involve positive powers of $\sigma^2(k)T$ and consequently that the limit $T \to 0$ is not singular. This may be consistent with the fact that the Novikov–Carini–Quadrio FRR with the small random forcing agrees well with the linear response function under the deterministic setting.

Appendix D. Short-time expansion of the Novikov–Carini–Quadrio FRR in Lagrangian coordinates

We consider the Taylor expansion of the Novikov–Carini–Quadrio FRR in Lagrangian coordinates at short times as in the previous Appendix C. In our DNS study we dealt with the Lagrangian response function only for the ordering, $t_\ell \geq t_m$. Here, we study theoretically both orderings, $t_\ell \geq t_m$ and $t_m \geq t_\ell$. In this Appendix D we first consider the latter ordering and then switch to the former, which is more complicated.

To be specific, we first consider the expansion for $t_\ell \leq t_m = t_\ell + \varepsilon$ ($\varepsilon \geq 0$)

$$
\begin{aligned}
G_{jj}^{(L,T)}&(\boldsymbol{k}, -\boldsymbol{k}, t_\ell \mid t_\ell + \varepsilon, t_\ell) \\
&= \frac{1}{3 \times 2\tilde{\sigma}^2(k)T} \langle \hat{v}_j(\boldsymbol{k}, t_\ell \mid t_\ell + \varepsilon)\hat{\zeta}_j(-\boldsymbol{k}, t_\ell \mid t_\ell)\rangle \\
&= \tilde{a}_0 + \tilde{a}_1\varepsilon + \tilde{a}_2\varepsilon^2 + \dots.
\end{aligned} \tag{D1}
$$

Here, we take summation over the index j. In what follows, we express the coefficients $\tilde{a}_0$, $\tilde{a}_1$ and $\tilde{a}_2$ in terms of the equal-time (at t_ℓ) correlation functions of the Eulerian velocity modes and discuss their dominant scaling behaviour as a function of k in the inertial range. We will show the dominant scaling is the Kolmogorov scaling, $\epsilon^{-1/3}k^{-2/3}$, in the inertial range.

The expansion procedure is the same as in the Eulerian case. However, one should be careful of where to add the noise. As discussed in Appendix B, the noise $\hat{\zeta}_j(\boldsymbol{k}, t_\ell \mid t_m)$ is added to the right-hand side of the measuring-time evolution equation of the Lagrangian velocity (B4), namely

$$
\begin{aligned}
\partial_{t_m}\hat{v}_j(\boldsymbol{k}, t_\ell \mid t_m) = &-(2\pi)^3 \nu \sum_{\boldsymbol{p}} p^2 \hat{u}_j(\boldsymbol{p}, t_m)\hat{\psi}(-\boldsymbol{p}, t_m \mid \boldsymbol{k}, t_\ell) \\
&- \mathrm{i}(2\pi)^3 \sum_{\boldsymbol{p}} \sum_{\substack{\boldsymbol{q},\boldsymbol{r} \\ \boldsymbol{q}+\boldsymbol{r}+\boldsymbol{p}=\boldsymbol{0}}} \frac{p_j p_a p_b}{p^2} \hat{u}_a(\boldsymbol{q}, t_m)\hat{u}_b(\boldsymbol{r}, t_m)\hat{\psi}(-\boldsymbol{p}, t_m \mid \boldsymbol{k}, t_\ell) \\
&+ (2\pi)^3 \sum_{\boldsymbol{p}} \hat{F}_j(\boldsymbol{p}, t_m)\hat{\psi}(-\boldsymbol{p}, t_m \mid \boldsymbol{k}, t_\ell) + \hat{\zeta}_j(\boldsymbol{k}, t_\ell \mid t_m).
\end{aligned} \tag{D2}
$$

Here, $\hat{\psi}(\boldsymbol{p}, t_m \mid \boldsymbol{q}, t_\ell)$ is the Fourier coefficient of the position function (Kaneda 1981). See also (B3). The formal Duhamel solution to (D2) is

$$
\hat{v}_j(\boldsymbol{k}, t_\ell \mid t_\ell + \varepsilon) = \hat{v}_j(\boldsymbol{k}, t_\ell \mid t_\ell) + \int_t^{t_\ell + \varepsilon} [\tilde{\Lambda}_j(\boldsymbol{k}, t_\ell \mid s) + \hat{\zeta}_j(\boldsymbol{k}, t_\ell \mid s)]\,\mathrm{d}s, \tag{D3}
$$

where $\tilde{\Lambda}_j(\boldsymbol{k}, t_\ell \mid t_m)$ denotes the first three terms on the right-hand side of (D2). Putting the solution into the velocity–noise correlation (D1), we have

$$
\langle \hat{v}_j(\boldsymbol{k}, t_\ell \mid t_\ell + \varepsilon)\hat{\zeta}_j(-\boldsymbol{k}, t_\ell \mid t_\ell)\rangle = 6\tilde{\sigma}^2(k)T + \int_{t_\ell}^{t_\ell + \varepsilon} \langle \tilde{\Lambda}_j(\boldsymbol{k}, t_\ell \mid s)\hat{\zeta}_j(-\boldsymbol{k}, t_\ell \mid t_\ell)\rangle\,\mathrm{d}s, \tag{D4}
$$

where we use $\langle \hat{v}_j(\boldsymbol{k}, t_\ell \mid t_\ell)\hat{\zeta}_j(-\boldsymbol{k}, t_\ell \mid t)\rangle = 0$ and the noise variance (B8) as we did in the Eulerian case.

To further calculate the correlation functions in (D4), we need the evolution equation of the Eulerian velocity since $\tilde{\Lambda}_j(\boldsymbol{k}, t_\ell \mid s)$ are written in terms of the Eulerian velocity.

The important point here is how the noise in (D2) is transformed in the equation of the Eulerian velocity. That can be obtained by multiplying (D2) by the position function and using (B6) as

$$\partial_{t_m}\hat{u}_j(\boldsymbol{k}, t_m) = \left(-\frac{\mathrm{i}}{2}\right) P_{jlm}(\boldsymbol{k}) \sum_{\substack{\boldsymbol{p},\boldsymbol{q} \\ \boldsymbol{p}+\boldsymbol{q}+\boldsymbol{k}=\boldsymbol{0}}} \hat{u}_l(-\boldsymbol{p}, t_m)\hat{u}_m(-\boldsymbol{q}, t_m) - \nu k^2 \hat{u}_j(\boldsymbol{k}, t_m)$$

$$+ \hat{F}_j(\boldsymbol{k}, t_m) + (2\pi)^3 P_{jl}(\boldsymbol{k}) \sum_{\boldsymbol{p}} \hat{\zeta}_l(\boldsymbol{p}, t_\ell \mid t_m)\hat{\psi}(\boldsymbol{k}, t_m \mid -\boldsymbol{p}, t_\ell). \tag{D5}$$

Here, the factor $(2\pi)^3$ is due to our normalisation of the Fourier modes of the position function.

From now on, we ignore the large-scale forcing $\hat{\boldsymbol{F}}$ and the viscous term to concentrate on the inertial-range scaling. We put the formal Duhamel solution of (D5) into the integrand of (D4). We also use the formal Duhamel solution of (B5) for the position function. Whenever $\hat{\boldsymbol{u}}(\boldsymbol{k}, s)$ or $\hat{\psi}(\boldsymbol{p}, s \mid \boldsymbol{q}, t_\ell)$ with $s \neq t_\ell$ appear in correlations, we replace them by the Duhamel expressions in order to express them with the equal-time correlations at time t_ℓ. We utilise the equal-time expression of the position function $\hat{\psi}(\boldsymbol{p}, t_\ell \mid \boldsymbol{q}, t_\ell) = \delta_{\boldsymbol{p},-\boldsymbol{q}}/(2\pi)^3$ as well. Most of the terms at ε^2 cancel due to the projection operator in the noise term in (D5). We then arrive at a rather simple result up to the second order (ε^2)

$$\langle \hat{v}_j(\boldsymbol{k}, t_\ell \mid t + \varepsilon)\hat{\zeta}_j(-\boldsymbol{k}, t_\ell \mid t)\rangle = 6\tilde{\sigma}^2(k)T$$

$$- 2\tilde{\sigma}^2(k)T\varepsilon^2 P_{jb}(\boldsymbol{k}) \sum_{\boldsymbol{p}} \frac{p_j p_a p_b p_c}{p^2} \langle \hat{u}_c(\boldsymbol{p} + \boldsymbol{k}, t_\ell)\hat{u}_a(-\boldsymbol{p} - \boldsymbol{k}, t_\ell)\rangle + O(\varepsilon^3). \tag{D6}$$

This yields the desired expression of the Lagrangian response function

$$G_{jj}^{(L,T)}(\boldsymbol{k}, -\boldsymbol{k}, t_\ell \mid t_\ell + \varepsilon, t_\ell) = 1 - \frac{\varepsilon^2}{3}k_a k_b \sum_{\boldsymbol{p}} \left(1 - \frac{(\boldsymbol{k} \cdot \boldsymbol{p})^2}{k^2 p^2}\right)$$

$$\times \langle \hat{u}_a^*(\boldsymbol{p} + \boldsymbol{k}, t_\ell)\hat{u}_b(\boldsymbol{p} + \boldsymbol{k}, t_\ell)\rangle + O(\varepsilon^3). \tag{D7}$$

Now we consider the leading scaling behaviour of the coefficient of the quadratic term of ε. To do this, we assume first that the diagonal components in (D7) are dominant, next, that the Kolmogorov energy spectrum holds, $\langle |\hat{\boldsymbol{u}}(\boldsymbol{k}, t_\ell)|^2\rangle = C_K/(2\pi)\epsilon^{2/3}k^{-11/3}$ for $k_0 \leq |\boldsymbol{k}| \leq k_1$ and, finally, that the summation can be approximated by an integral. These assumptions lead to the following leading behaviour for $k_0 \ll k \ll k_1$:

$$k_a k_b \sum_{\boldsymbol{p}} \left(1 - \frac{(\boldsymbol{k} \cdot \boldsymbol{p})^2}{k^2 p^2}\right) \langle \hat{u}_a^*(\boldsymbol{p} + \boldsymbol{k}, t_\ell)\hat{u}_b(\boldsymbol{p} + \boldsymbol{k}, t_\ell)\rangle$$

$$\simeq \frac{C_K}{6\pi}\epsilon^{2/3}k^2 \sum_{\boldsymbol{p}} \left(1 - \frac{(\boldsymbol{k} \cdot \boldsymbol{p})^2}{k^2 p^2}\right) |\boldsymbol{k} + \boldsymbol{p}|^{-11/3}$$

$$\simeq \frac{C_K}{6\pi}\epsilon^{2/3}k^2 \left(\frac{L}{2\pi}\right)^3 \int_{k_0}^{k_1} \mathrm{d}p \int_0^\pi \mathrm{d}\theta \int_0^{2\pi} \mathrm{d}\varphi\, p^2 \sin^3\theta (k^2 + p^2 + 2kp\cos\theta)^{-11/6}$$

$$= \frac{6\sqrt{3}}{35}\pi C_K\epsilon^{2/3}k^{4/3} + \text{(subleading terms)}, \tag{D8}$$

where the integral can be calculated analytically.

Finally, the Lagrangian response function at short time is expressed as

$$G_{jj}^{(L,T)}(\boldsymbol{k}, -\boldsymbol{k}, t_\ell \mid t_\ell + \varepsilon, t_\ell) \simeq 1 - \varepsilon^2 \frac{2\sqrt{3}}{35} \pi C_K \epsilon^{2/3} k^{4/3} + O(\varepsilon^3). \qquad (D9)$$

Therefore, the time scale of the Lagrangian response function at short time is given by the Kolmogorov temporal scaling $\epsilon^{-1/3} k^{-2/3}$, as expected. The result (D9) can be compared with the result of the LRA in Kaneda *et al.* (1999), $G^{(L,T=0)} = 1 - 0.530 C_K \epsilon^{2/3} k^{4/3} \varepsilon^2 + O(\varepsilon^3)$. The numerical constant in (D9), namely $(2\sqrt{3}/35)\pi \simeq 0.311$, is smaller than that of the LRA result.

Next, let us consider the Lagrangian response function with the ordering $t_\ell \geq t_m$, which is the same ordering considered in our numerical study in § 3. Specifically, setting $t_\ell = t_m + \varepsilon(\varepsilon \geq 0)$, the short-time expansion is

$$
\begin{aligned}
G_{jj}^{(L,T)}(\boldsymbol{k}, -\boldsymbol{k}, t_m + \varepsilon \mid t_m + \varepsilon, t_m) &= \frac{1}{4\tilde{\sigma}^2(k)T} \langle \hat{v}_j(\boldsymbol{k}, t_m + \varepsilon \mid t_m + \varepsilon) \hat{\zeta}_j(-\boldsymbol{k}, t_m + \varepsilon \mid t_m) \rangle \\
&= \frac{1}{4\tilde{\sigma}^2(k)T} \langle \hat{u}_j(\boldsymbol{k}, t_m + \varepsilon) \hat{\zeta}_j(-\boldsymbol{k}, t_m + \varepsilon \mid t_m) \rangle \\
&= \tilde{b}_0 + \tilde{b}_1 \varepsilon + \tilde{b}_2 \varepsilon^2 + \dots . \qquad (D10)
\end{aligned}
$$

The factor 4 in the denominator is due to the incompressibility, as we will see. We wish to write the coefficients $\tilde{b}_0$, $\tilde{b}_1$ and $\tilde{b}_2$ in terms of the Eulerian velocity modes.

To evaluate the velocity–noise correlation, we need the labelling-time evolution of the random forcing, which is described by the passive vector equation. Hence, its Duhamel solution is

$$\hat{\zeta}_j(\boldsymbol{k}, t_m + \varepsilon \mid t_m) = \hat{\zeta}_j(\boldsymbol{k}, t_m \mid t_m) - \mathrm{i}k_a \int_{t_m}^{t_m+\varepsilon} \sum_{\substack{\boldsymbol{p},\boldsymbol{q} \\ \boldsymbol{p}+\boldsymbol{q}+\boldsymbol{k}=0}} \hat{u}_a(-\boldsymbol{p}, s) \hat{\zeta}_j(-\boldsymbol{q}, s \mid t_m) \, \mathrm{d}s. \qquad (D11)$$

Similarly, we use the formal solution of the Eulerian velocity to (D5),

$$
\begin{aligned}
\hat{u}_j(\boldsymbol{k}, s) = \hat{v}_j(\boldsymbol{k}, s \mid s) &= \hat{u}_j(\boldsymbol{k}, t_m) \\
&+ \int_{t_m}^{s} \mathrm{d}s_1 \left[\Lambda_j(\boldsymbol{k}, s_1) + (2\pi)^3 P_{ja}(\boldsymbol{k}) \sum_{\boldsymbol{p}} \hat{\zeta}_a(\boldsymbol{p}, s \mid s_1) \hat{\psi}(\boldsymbol{k}, s_1 \mid -\boldsymbol{p}, s) \right]. \qquad (D12)
\end{aligned}
$$

Notice that we set the labelling time appearing on the right-hand side of (D12) to the same time on the left-hand side. Here again, we ignore the viscous term and the large-scale forcing. We also need the formal solution of the labelling-time evolution of the position function

$$\hat{\psi}(\boldsymbol{k}', t_m \mid \boldsymbol{k}, t_m + \varepsilon) = \hat{\psi}(\boldsymbol{k}', t_m \mid \boldsymbol{k}, t_m) - \mathrm{i}k_a \int_{t_m}^{t_m+\varepsilon} \mathrm{d}s \sum_{\substack{\boldsymbol{p},\boldsymbol{q} \\ \boldsymbol{p}+\boldsymbol{q}+\boldsymbol{k}=0}} \hat{u}_a(-\boldsymbol{p}, s) \hat{\psi}(\boldsymbol{k}', t_m \mid -\boldsymbol{q}, s). \qquad (D13)$$

Using (D11)–(D13) successively, the velocity–noise correlation in (D10) can be calculated as

$$\langle \hat{v}_j(\boldsymbol{k}, t_m + \varepsilon \mid t_m + \varepsilon) \hat{\xi}_j^*(\boldsymbol{k}, t_m + \varepsilon \mid t_m) \rangle = 4\sigma^2(k)T$$

$$- \sigma^2(k)T\varepsilon^2 \left[6k_b k_d \sum_{\boldsymbol{p}} \langle \hat{u}_b^*(\boldsymbol{p}, t_m) \hat{u}_d(\boldsymbol{p}, t_m) \rangle \right.$$

$$+ k_b \langle \hat{u}_j(\boldsymbol{k}, t_m) \hat{u}_c^*(\boldsymbol{k}, t_m) \rangle \sum_{\boldsymbol{p}} P_{bcd}(-\boldsymbol{p}) P_{dj}(\boldsymbol{k} + \boldsymbol{p})$$

$$\left. + P_{jab}(\boldsymbol{k}) \sum_{\boldsymbol{p}} \{ P_{bcj}(\boldsymbol{p} + \boldsymbol{k}) - 2k_c P_{bj}(\boldsymbol{p} + \boldsymbol{k}) \} \times \langle \hat{u}_a^*(\boldsymbol{p}, t_m) \hat{u}_c(\boldsymbol{p}, t_m) \rangle \right] + O(\varepsilon^3).$$

(D14)

Now we again assume that the dominant part is the diagonal components of the second-order velocity correlations. This leads to the expansion of the response function

$$G_{jj}^{(L,T)}(\boldsymbol{k}, -\boldsymbol{k}, t_m + \varepsilon \mid t_m + \varepsilon, t_m) \simeq 1 - \frac{\varepsilon^2}{6} \left[4k^2 \langle E \rangle + \frac{1}{2} \langle |\hat{\boldsymbol{u}}(\boldsymbol{k}, t_m)|^2 \rangle \right.$$

$$\left. \times \sum_{\boldsymbol{p}} \frac{\{\boldsymbol{k} \cdot (\boldsymbol{k} + \boldsymbol{p})\}\{\boldsymbol{p} \cdot (\boldsymbol{p} + 2\boldsymbol{k})\}}{|\boldsymbol{k} + \boldsymbol{p}|^2} - \sum_{\boldsymbol{p}} (\boldsymbol{p} \cdot \boldsymbol{k}) \langle |\hat{\boldsymbol{u}}(\boldsymbol{p}, t_m)|^2 \rangle \right] + O(\varepsilon^3). \quad \text{(D15)}$$

The last term in the ε^2 coefficient vanishes. The second term can be estimated by approximating it with the integral

$$\sum_{\boldsymbol{p}} \frac{\{\boldsymbol{k} \cdot (\boldsymbol{k} + \boldsymbol{p})\}\{\boldsymbol{p} \cdot (\boldsymbol{p} + 2\boldsymbol{k})\}}{|\boldsymbol{k} + \boldsymbol{p}|^2} \simeq \left(\frac{L}{2\pi} \right)^3 \int \mathrm{d}\boldsymbol{p} \frac{(k^2 + \boldsymbol{k} \cdot \boldsymbol{p})(p^2 + 2\boldsymbol{k} \cdot \boldsymbol{p})}{|\boldsymbol{k} + \boldsymbol{p}|^2}$$

$$= 2\pi k \int_{k_0}^{k_1} \mathrm{d}p p^3 \int_0^\pi \mathrm{d}\theta \, \sin\theta \frac{(k + p\cos\theta)(p + 2k\cos\theta)}{k^2 + p^2 + 2kp\cos\theta}$$

$$= \frac{2}{3}\pi k^2 k_1^3 + 2\pi k^3 k_1 + \text{(subleading terms)}.$$

Here, we have dependence on the high-wavenumber cutoff $k_1 (\gg k)$. Therefore, the linear response function is written as

$$G_{jj}^{(L,T)}(\boldsymbol{k}, -\boldsymbol{k}, t_m + \varepsilon | t_m + \varepsilon, t_m) \sim 1 - \frac{\varepsilon^2}{6} \left[4k^2 \langle E \rangle + \frac{1}{6} C_K \epsilon^{2/3} k^{-5/3} k_1^3 + \dots \right] + O(\varepsilon^3). \quad \text{(D16)}$$

In this case, the dominant time scale of the linear response function is $\epsilon^{-1/3} k^{5/6} k_1^{-3/2} = \epsilon^{-1/3} k_1^{-2/3} (k/k_1)^{5/6}$, which is an unexpected result. So far, we do not have a clear interpretation of this time scale. Nevertheless, this manifests non-locality, which can be ascribed to the position function. In fact, the k_1 dependence comes from the correlation between the velocity and the advection term in (D11). Although the wavenumber k which we are now probing is much less than k_1, the time scale determined by k_1 (the highest active wavenumber of the velocity) is a reminiscent of the viscous–convective-range picture of the passive scalar transport at high Schmidt numbers, see, e.g. Davidson (2004).

919 A9-40

Here, we notice that the scaling behaviour obtained above cannot be compared with our DNS result described in § 3, since our simulation did not have sufficient scale separation, $k_0 \ll k \ll k_1$, between the beginning and the ending wavenumbers of the inertial range. Nevertheless, we comment on the short-time behaviour of the Lagrangian response function observed in DNS shown in § 3. As shown in figure 7, the Lagrangian response functions for large wavenumbers ($k_\eta/16$ and $k_\eta/32$) at short times are so flat that the parabolic decrease does not fit well. If we plot $1 - G^L(k, t_\ell - t_m)$ as a function of $t_\ell - t_m$ in log–log coordinates, the short-time part is almost flat for $k_\eta/32$ and is close to $(t_\ell - t_m)^{0.50}$ for $k_\eta/16$. We speculate that these apparent scaling behaviours are caused by the large-scale forcing (2.2) and by some competition between the ε and ε^2 terms of the short-time Taylor expansion.

Appendix E. The p.d.f.s of Eulerian and Lagrangian velocity Fourier modes

In this section, with our numerical data, we show that p.d.f.s of the velocity Fourier modes are self-similar and close to Gaussian. In particular, this holds not only for the Eulerian velocity, but also for the Lagrangian-history velocity. For the Eulerian velocity, we consider both cases with and without the random noise $\boldsymbol{\xi}(\boldsymbol{k}, t)$ in (2.10). The setting of the noise is the same as in § 2.3, namely $\sigma(k) = k^{-1}$ and $T = 10^{-6}$. For the Lagrangian velocity, we consider only the case without the noise.

To calculate the p.d.f. of the Eulerian velocity modes, we consider a shell in the wavenumber space, $k \leq |\boldsymbol{k}| < k + \Delta k$ with $\Delta k = 1$, as we do in calculating the energy spectrum. Within this shell characterised with k, we calculate the p.d.f. of the real part of the φ-component of the Fourier mode, $\mathrm{Re}[\hat{u}_\varphi(\boldsymbol{k}, t)]$. We take 10 snapshots in the statistically steady state, starting from different initial conditions. The real parts are then standardised to have zero mean and unit standard deviation. The resultant p.d.f.s shown in figure 13 for five different wavenumber shells indicate that they are self-similar and close to Gaussian. This is in stark contrast to behaviour of p.d.f.s for the Eulerian velocity increments in physical space, which are neither self-similar nor Gaussian, see, e.g. Frisch (1996).

To estimate quantitatively how close they are to Gaussian, we calculate the skewness and kurtosis, which are defined respectively as the third and fourth moments of the standardised variables. The results listed in table 1 are indeed around those of the Gaussian distribution, although the smallest- and largest-wavenumber cases in table 1 have somewhat larger kurtosis. Similar results are obtained for the imaginary parts of the φ-components and both parts of the θ-components of the Eulerian velocity modes (figure not shown).

For the Lagrangian-history velocity, we use the same method to calculate the p.d.f.s as in the Eulerian case. However, it should be noted that the Lagrangian-history velocity, $\hat{\boldsymbol{v}}(\boldsymbol{k}, t_\ell \mid t_m)(t_\ell \geq t_m)$, is not statistically steady and that it is not solenoidal in general, $\boldsymbol{k} \cdot \hat{\boldsymbol{v}}(\boldsymbol{k}, t_\ell \mid t_m) \neq 0$. Hence, the decomposition of the Lagrangian mode has three components as

$$\hat{\boldsymbol{v}}(\boldsymbol{k}, t_\ell \mid t_m) = \hat{v}_\varphi(\boldsymbol{k}, t_\ell \mid t_m)\boldsymbol{e}_\varphi + \hat{v}_\theta(\boldsymbol{k}, t_\ell \mid t_m)\boldsymbol{e}_\theta + \hat{v}_c(\boldsymbol{k}, t_\ell \mid t_m)\hat{\boldsymbol{k}}, \tag{E1}$$

in contrast to the Eulerian mode given in (2.4) with two components. Here, $\hat{\boldsymbol{k}} = \boldsymbol{k}/|\boldsymbol{k}|$ and $\hat{v}_c$ is the compressible component, which is zero at $t_\ell = t_m$.

We calculate p.d.f.s of the real and imaginary parts of the three components at 11 different instances, $t_\ell = t_m + 0.05\tau_{to}, t_m + 0.1\tau_{to}, t_m + 0.2\tau_{to}, \ldots, t_m + \tau_{to}$. We use the same 10 snapshots (as we used in the Eulerian case) as the initial Lagrangian velocity
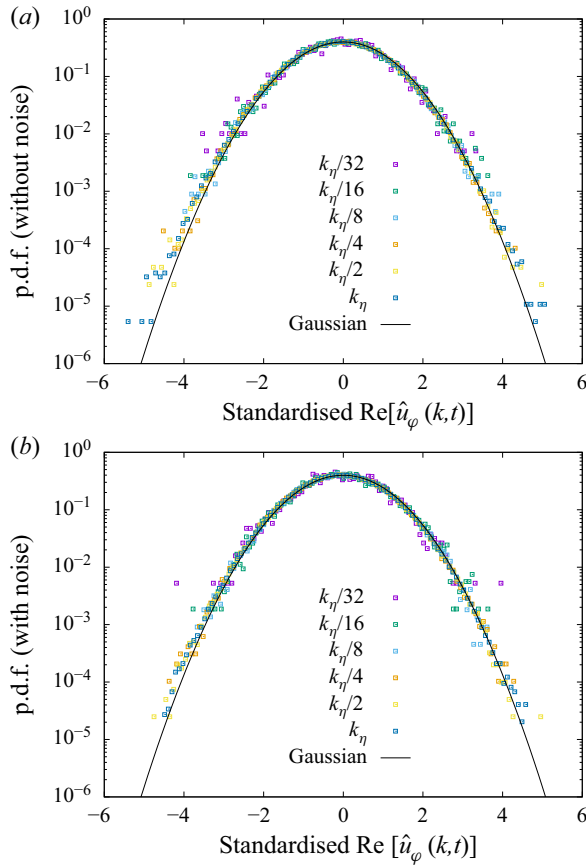
Figure 13. The p.d.f.s of the real parts of the Eulerian velocity Fourier modes, $\text{Re}[\hat{u}_\varphi(\boldsymbol{k}, t)]$, for $R_\lambda = 210(k_\eta = 160)$: (a) without the random noise, or equivalently $T = 0$; (b) with the random noise.

Shell wavenumber	Skewness		Kurtosis	
	(without noise)	(with noise)	(without noise)	(with noise)
$k_\eta/32$	-1.09×10^{-1}	-5.70×10^{-2}	3.19	3.16
$k_\eta/16$	1.75×10^{-2}	4.30×10^{-2}	3.08	3.00
$k_\eta/8$	-7.89×10^{-3}	1.06×10^{-2}	3.05	3.02
$k_\eta/4$	-1.42×10^{-2}	-9.03×10^{-3}	3.04	3.03
$k_\eta/2$	2.50×10^{-3}	3.06×10^{-4}	3.05	3.05
k_η	9.80×10^{-4}	-3.98×10^{-3}	3.11	3.05

Table 1. Skewness and kurtosis of the real part of the Eulerian velocity Fourier mode, $\text{Re}[\hat{u}_\varphi(\boldsymbol{k}, t)]$, for $R_\lambda = 210(k_\eta = 160)$ with and without the random noise. For Gaussian random variables, the skewness is zero and the kurtosis is 3.

fields ($t_\ell = t_m$) for the passive vector equations (3.1). In figure 14, we plot p.d.f.s of the real parts of the compressible components at two particular instances $t_\ell = t_m + 0.05\tau_{to}$ and $t_m + 0.50\tau_{to}$. We choose this component since it may behave differently from the solenoidal Eulerian modes, $\hat{u}_\varphi$ and $\hat{u}_\theta$. Although the compressible components are zero at
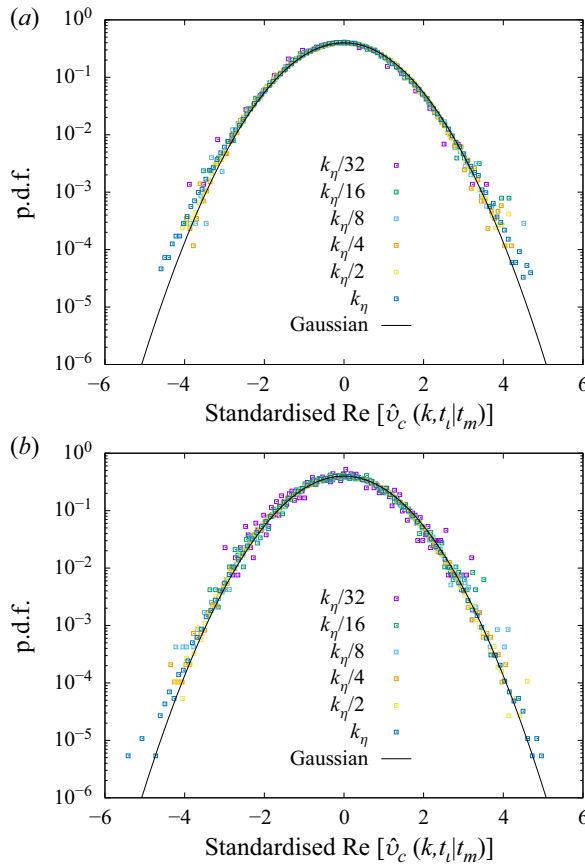
Figure 14. The p.d.f.s of the real parts of the Lagrangian velocity Fourier modes, $\mathrm{Re}[\hat{v}_c(\boldsymbol{k}, t_\ell \mid t_m)]$, for $R_\lambda = 210(k_\eta = 160)$; (a) $t_\ell = t_m + 0.05\tau_{to}$, (b) $t_\ell = t_m + 0.50\tau_{to}$.

Shell wavenumber	Skewness		Kurtosis	
	$(t_\ell = t_m + 0.05\tau_{to})$	$(t_m + 0.5\tau_{to})$	$(t_m + 0.05\tau_{to})$	$(t_m + 0.50\tau_m)$
$k_\eta/32$	3.77×10^{-2}	-2.92×10^{-2}	3.08	3.05
$k_\eta/16$	3.64×10^{-2}	-7.28×10^{-3}	3.07	3.13
$k_\eta/8$	7.60×10^{-3}	2.57×10^{-2}	3.04	3.07
$k_\eta/4$	-1.14×10^{-2}	-8.68×10^{-3}	3.02	3.01
$k_\eta/2$	2.82×10^{-3}	-1.03×10^{-2}	3.05	3.02
k_η	-1.35×10^{-3}	-1.85×10^{-3}	3.16	3.04

Table 2. Skewness and kurtosis of the real part of the Lagrangian velocity Fourier mode, $\mathrm{Re}[\hat{v}_c(\boldsymbol{k}, t_\ell \mid t_m)]$ at $t_\ell = t_m + 0.05\tau_{to}$ and $t_m + 0.50\tau_{to}$ for $R_\lambda = 210(k_\eta = 160)$.

$t_\ell = t_m$, they quickly develop and their p.d.f.s become self-similar and close to Gaussian at $t_\ell = t_m + 0.05\tau_{to}$ as shown in figure 14 (how they develop to Gaussian from zero is beyond the scope of this paper). We observe small differences between the two times shown in figure 14 including that the earlier time p.d.f.s have less developed tails and less fluctuations. The p.d.f.s of the imaginary parts of the compressible component behave

in a similar manner. Both real and imaginary parts of the φ- and θ-components at both times are also similar to those at $t_\ell = t_m + 0.50\tau_{to}$ shown in figure 14. To observe how close the p.d.f.s are to Gaussian, we list skewness and kurtosis of $\mathrm{Re}[\hat{v}_c(\boldsymbol{k}, t_\ell \mid t_m)]$ in table 2. Similar results are obtained for another part of the same components and both parts of the other components at other instances. In conclusion, we observe that the p.d.f.s of the Eulerian and Lagrangian-history velocity Fourier modes are close to Gaussian in the inertial and dissipation ranges. Thus we have verified, for $R_\lambda = 210$, the same Gaussianity of the Eulerian velocity modes as have been numerically found for $R_\lambda = 80$ by Brun & Pumir (2001).

REFERENCES

BIFERALE, L., DAUMONT, I., LACORATA, G. & VULPIANI, A. 2001 Fluctuation-response relation in turbulent systems. *Phys. Rev.* E **65** (1), 016302.

BRUN, C. & PUMIR, A. 2001 Statistics of fourier modes in a turbulent flow. *Phys. Rev.* E **63** (5), 056313.

CARDY, J. 1996 *Scaling and Renormalization in Statistical Physics*. Cambridge University Press.

CARINI, M. & QUADRIO, M. 2010 Direct-numerical-simulation-based measurement of the mean impulse response of homogeneous isotropic turbulence. *Phys. Rev.* E **82**, 066301.

CUGLIANDOLO, L.F., KURCHAN, J. & PARISI, G. 1994 Off equilibrium dynamics and aging in unfrustrated systems. *J. Phys. I (France)* **4**, 1641.

DAVIDSON, P.A. 2004 *Turbulence*. Oxford University Press.

EYINK, G.L. & FRISCH, U. 2011 Robert H. Kraichnan. In *A Voyage Through Turbulence* (ed. Y. Kaneda, P.A. Davidson & K.R. Sreenivasan), pp. 329–372. Cambridge University Press.

FORSTER, D., NELSON, D.R. & STEPHEN, M.J. 1977 Large-distance and long-time properties of a randomly stirred fluid. *Phys. Rev.* A **16** (2), 732.

FRISCH, U. 1996 *Turbulence*. Cambridge University Press.

GOTOH, T., ROGALLO, R.S., HERRING, J.R. & KRAICHNAN, R.H. 1993 Lagrangian velocity correlations in homogeneous isotropic turbulence. *Phys. Fluids* A **5** (11), 2846.

HARADA, T. & SASA, S.-I. 2005 Equality connecting energy dissipation with a violation of the fluctuation-response relation. *Phys. Rev. Lett.* **95**, 130602.

HARADA, T. & SASA, S.-I. 2006 Energy dissipation and violation of the fluctuation-response relation in nonequilibrium Langevin systems. *Phys. Rev.* E **73**, 026131.

HE, G., JIN, G. & YANG, Y. 2017 Space-time correlations and dynamics coupling in turbulent flows. *Annu. Rev. Fluid Mech.* **49**, 51–70.

KANEDA, Y. 1981 Renormalized expansions in the theory of turbulence with the use of the Lagrangian position function. *J. Fluid Mech.* **107**, 131–145.

KANEDA, Y. 1993 Lagrangian and Eulerian time correlations in turbulence. *Phys. Fluids* A **5** (11), 2835–2845.

KANEDA, Y. 2007 Lagrangian renormalized approximation of turbulence. *Fluid Dyn. Res.* **39** (7), 526–551.

KANEDA, Y. & GOTOH, T. 1991 Lagrangian velocity autocorrelation in isotropic turbulence. *Phys. Fluids* A **3** (8), 1924.

KANEDA, Y., ISHIHARA, T. & GOTOH, K. 1999 Taylor expansions in powers of time of lagrangian and Eulerian two-point two-time velocity correlations in turbulence. *Phys. Fluids* **11**, 2154–2166.

KIDA, S. & GOTO, S. 1997 A Lagrangian direct-interaction approximation for homogeneous isotropic turbulence. *J. Fluid Mech.* **345**, 307–345.

KRAICHNAN, R.H. 1959 The structure of isotropic turbulence at very high Reynolds numbers. *J. Fluid Mech.* **5**, 497–543.

KRAICHNAN, R.H. 1964*a* Decay of isotropic turbulence in the direct-interaction approximation. *Phys. Fluids* **7**, 1030–1048.

KRAICHNAN, R.H. 1964*b* Kolmogorov's hypotheses and Eulerian turbulence theory. *Phys. Fluids* **7** (11), 1723.

KRAICHNAN, R.H. 1965 Lagrangian–history closure approximation for turbulence. *Phys. Fluids* **8**, 575.

KRAICHNAN, R.H. 1966 Isotropic turbulence and inertial-range structure. *Phys. Fluids* **9**, 1728–1752.

LESLIE, D.C. 1973 *Developments in the Theory of Turbulence*. Clarendon Press.

LUCHINI, P., QUADRIO, M. & ZUCCHER, S. 2006 The phase-locked mean impulse response of a turbulent channel flow. *Phys. Fluids* **18**, 121702.

MARCONI, U.M.B., PUGLISI, A., RONDONI, L. & VULPIANI, A. 2008 Fluctuation–dissipation: response theory in statistical physics. *Phys. Rep.* **461**, 111–195.

MATSUMOTO, T., OTSUKI, M., OOSHIDA, T., GOTO, S. & NAKAHARA, A. 2014 Response function of turbulence computed via fluctuation-response relation of a Langevin system with vanishing noise. *Phys. Rev.* E **89**, 061002(R).

MIYAZAKI, K. & REICHMAN, D.R. 2005 Mode-coupling theory and the fluctuation–dissipation theorem for nonlinear Langevin equations with multiplicative noise. *J. Phys.* A **38** (20), L343–L355.

NOVIKOV, E.A. 1965 Functionals and the random-force method in turbulence theory. *Sov. Phys. JETP* **20**, 1290–1294.

POPE, S.B. 2000 *Turbulent Flows*. Cambridge University Press.

PUGLISI, A., SARRACINO, A. & VULPIANI, A. 2017 Temperature in and out of equilibrium: a review of concepts, tools and attempts. *Phys. Rep.* **709–710**, 1–60.

REICHMAN, D.R. & CHARBONNEAU, P. 2005 Mode-coupling theory. *J. Stat. Mech.* **2005** (5), P05013.

SAGAUT, P. & CAMBON, C. 2008 *Homogeneous Turbulence Dynamics*. Cambridge University Press.

SAIN, A., MANU, & PANDIT, R. 1998 Turbulence and multiscaling in the randomly forced Navier–Stokes equation. *Phys. Rev. Lett.* **81** (20), 4377.

YEUNG, P.K. & POPE, S.B. 1989 Lagrangian statistics from direct numerical simulations of isotropic turbulence. *J. Fluid Mech.* **207**, 531–586.

ZINN-JUSTIN, J. 2002 *Quantum Field Theory and Critical Phenomena*. Oxford University Press.